ERDC/CHL TR-XX-DRAFT

Coastal and Hydraulics Laboratory

US Army Corps of Engineers®
Engineer Research and Development Center

ERDC
ENGINEER RESEARCH & DEVELOPMENT CENTER

Coastal Ocean Data Systems (CODS) and Coastal Inlets Research Program (CIRP)

Quantifying Coastal Evolution and Project Performance at Beaches Using Satellite Imagery

Ian W. Conery, Nicholas R. Olsen, Shannon Brown and Katherine L. Brodie

September 2022

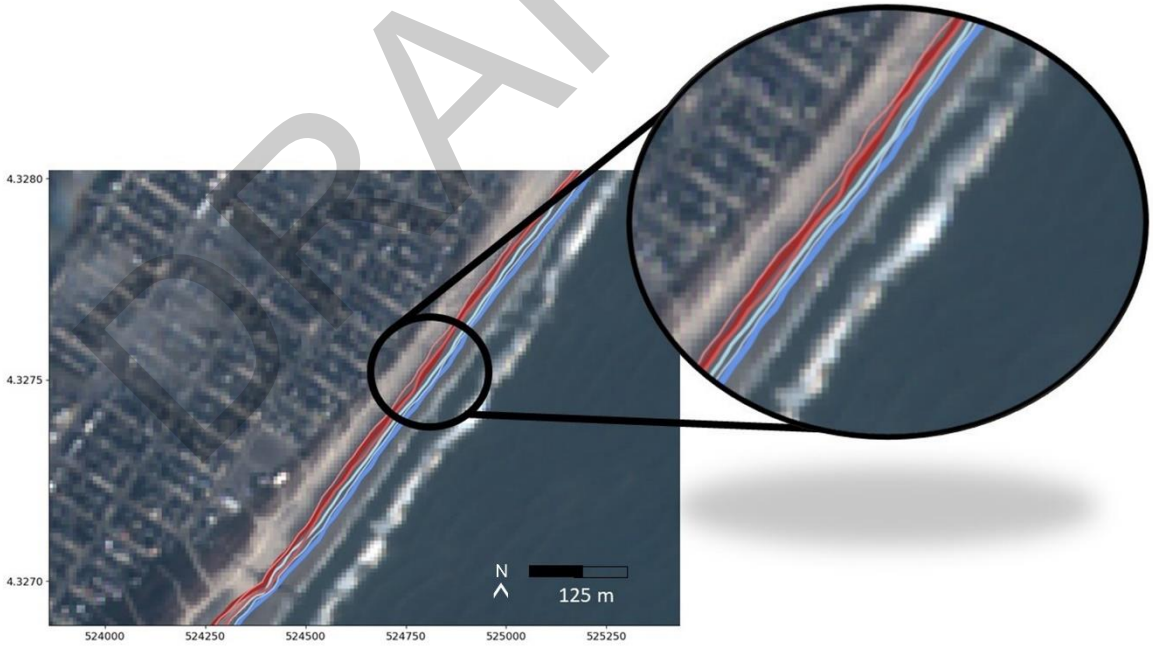

Program Title [[[If project was not funded by a military or civil program, delete all text in this cell]]]

ERDC/CHL TR-XX-DRAFT
Month Year

Quantifying Coastal Evolution and Project Performance at Beaches Using Satellite Imagery (Report Template v4.02)

Ian W. Conery, Nicholas R. Olsen, Shannon Brown and Katherine L. Brodie

Coastal and Hydraulics Laboratory
U.S. Army Engineer Research and Development Center
3909 Halls Ferry Road
Vicksburg, MS 39180

Final report

Prepared for Coastal and Ocean Data Systems; Coastal Inlets Research Program

Under Project ####, "CODS/CIRP CoastSat"

Monitored by Coastal and Hydraulics Laboratory
U.S. Army Engineer Research and Development Center
Vicksburg, MS 39180-6199

Abstract

Accurately delineating the shoreline is crucial for tracking coastal evolution, community vulnerability, storm impacts/recovery, and for coastal management decision making. However, existing shoreline measurement methods are often time-consuming and expensive and therefore, USACE Districts are often forced to narrow areas of interest or monitoring frequency, decreasing the likelihood of making data-driven management decisions, especially over regional scales. In the last decade, space-borne earth observations have captured images sub-weekly, and can potentially be used for shoreline monitoring. This work investigated the Python-based CoastSat toolkit and compared the shorelines derived from publicly available satellite imagery to ground truth surveys at 37 sites across the nation chosen in coordination with Districts. Mean horizontal errors ranged from 4.21 to 20.58 m with an overall mean of 11.32 m. Sentinel-2 had the highest individual accuracy at 8.86 m. Tidal corrections improved accuracies at 82% of sites. The CoastSat slope function was tested and there were negligible differences in shoreline accuracy when compared with user-defined slopes. Runup corrections improved satellite-derived shoreline accuracy at three of five tested sites, but further work is needed across more sites. Twenty-year satellite-derived trends generally align well with ground truth trends. This satellite-derived shoreline approach represents a powerful, free data source for Districts which is available at broad spatial and temporal scales. In particular, the satellite approach identified quantifying storm impacts/recovery, beach nourishment equilibration, diffusion and decay, shoreline response to nearshore berm placements and decadal shoreline evolution at the evaluated district sites. Work is ongoing to transition to a user-friendly software tool.

Contents

Figures and Tables

Figures

Tables

Preface

This study was conducted for the U.S. Army Corps of Engineers (USACE) Coastal Ocean Data Systems and Coastal Inlets Research Program under [[[Funding information from title page/Form 7]]]. The technical director was Julie Rosati.

The work was performed by the Coastal Observations and Analysis Branch and Hydrologic Systems Branch of the Flood and Coastal Division, U.S. Army Engineer Research and Development Center, Coastal and Hydraulics Laboratory (ERDC-CHL). At the time of publication, Erin Diurba and Pearce Chang were chiefs; Lauren Dunkin was Acting Chief, Flood and Coastal Division; and Julie Rosati was the Technical Director for Flood and Coastal Division. The Deputy Director of ERDC-CHL was Keith Flowers, and the Director was Ty Wamsley.

The Commander of ERDC was COL Christian Patterson, and the Director was Dr. David W. Pittman.

1 Introduction

Coastal areas across the nation contain valuable historical, cultural, and natural resources that generate billions of dollars annually through tourism and industry (e.g., shipping and fishing). The position of the shoreline, generally defined as the land-sea interface, is a critical metric that is often utilized to track coastal evolution, community vulnerability, storm impacts/recovery, and for coastal management decision making. Therefore, accurate delineation of the shoreline is crucial for coastal management decision making (e.g., establishing construction setbacks). Yet, shorelines are complex and fluctuate on scales from seconds to decades, making measurements and predictions quite challenging.

1.1 Background

Within USACE, frequent surveying of beaches and inlets is essential for understanding the relevant physical processes influencing sediment management and developing adaptive management strategies. Existing shoreline mapping techniques include GPS systems, airborne and terrestrial lidar, coastal video imaging and unmanned aerial systems. However, these existing methods are often time-consuming and expensive and therefore, to conserve limited operational resources (e.g., personnel and vessels), USACE Districts are often forced to narrow areas of interest or monitoring frequency, decreasing the likelihood of making data-driven management decisions. In the last decade, space-borne earth observations have captured images sub-weekly and can potentially be used to examine regional shoreline and inlet dynamics over sub-seasonal to multi-year time scales (e.g., Luijendijk et al., 2018; Xu, 2018; Hagenaars et al., 2018, Bergsma et al., 2020). NASA launched Landsat 5 in 1984 offering advantageous long-term shoreline change context, and numerous global satellite missions with improved optical imaging sensors have since followed (Fig. 1). Coastal data extraction from existing satellite observations would effectively incur no cost since the satellite imagery is publicly available, making it a low commitment choice for examining shoreline variability and preliminary planning for districts managing beach projects (e.g., Coastal Storm Risk Management) or inlets.

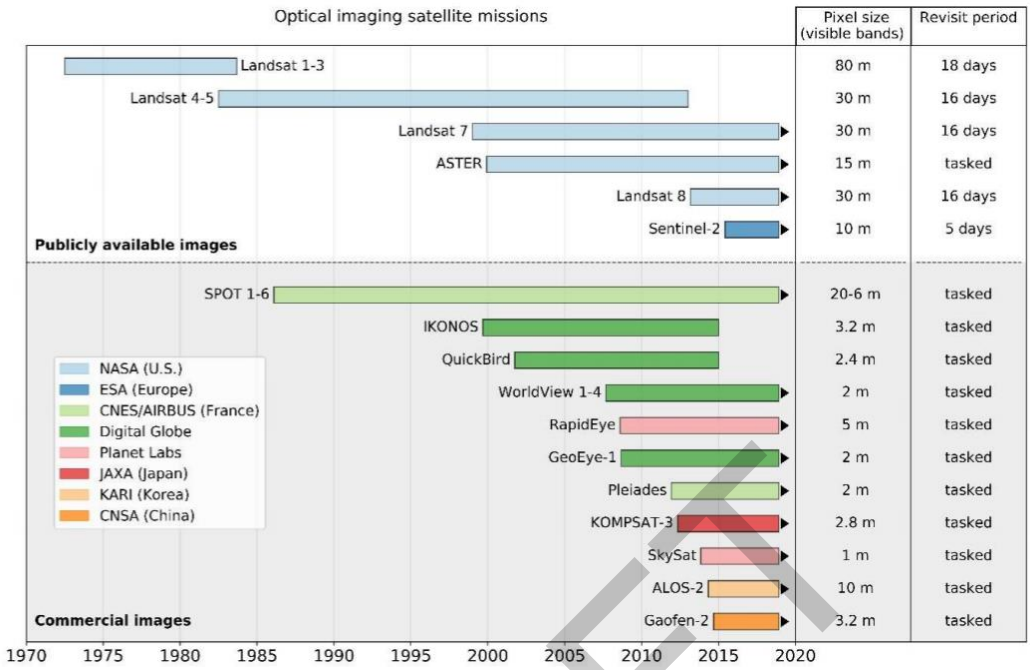

Figure 1. Major global civilian satellites and respective timelines (from Vos et al., 2019).

Using the normalized difference water index (NDWI) and machine learning algorithms, researchers have explored automated delineation of the boundary between land and sea in satellite imagery (Luijendijk et al 2018, Hagenaars et al 2018). Success led to development of an open-source algorithm known as CoastSat which uses a supervised Multi-Layer Perceptron algorithm to classify four regions in a coastal image: 'water', 'white-water', 'sand', and 'other land features' and from these classifications defines the shoreline as the instantaneous interface between water and sand (Vos et al., 2019). CoastSat has been used to generate time series of coastlines around the world, providing insight into shoreline position (e.g. Vos et al., 2019) and beach slope (Vos et al., 2020). The CoastSat algorithm exists as a Python algorithm, which is not easily or efficiently accessible to most district users, thereby motivating the creation of a more user-friendly, transferable shoreline mapping tool. In addition, the algorithm has not yet been evaluated on many managed coastlines and so the ability to resolve rapid profile changes associated with nourishments needs to be rigorously investigated.

Development of this satellite-based tool offers the opportunity to both analyze and quantify natural coastal processes as well as the impacts of

historic and future management strategies, such as nearshore berm placement and beach nourishments, on shoreline erosion rates at regional to national scales. Furthermore, these data could also be used to help inform future survey extent and/or timing, or act as a supplement to typical crewed surveys or planned airborne lidar surveys, especially in remote or hazardous regions (e.g., SAJ - Puerto Rico). Shallow coastal inlets are notoriously dynamic (e.g., Velasquez-Montoya et al., 2020) and can be hazardous to navigate (e.g., recreational boating), due to varying sediment exchanges and shoaling–processes which could be detectable from satellite data.

1.2 Objectives

The specific objectives of this overall effort are to 1) assess the ability of CoastSat to accurately quantify instantaneous shoreline positions and shoreline trends at a variety of USACE District sites by comparing to traditional ground-based survey methods and to 2) package the python-based satellite tool into a more user-friendly GIS tool for Districts (FY 23). In this report we focus on documenting the results of objective (1).

1.3 Approach

The remainder of this report will encompass 1) background on methodology (CoastSat and ERDC modifications), 2) test site and ground truth data descriptions, 3) instantaneous satellite shoreline accuracies compared to ground truth data, 4) long-term satellite shoreline trends, management applications and storm impacts/recovery and 5) conclusions and recommendations.

2 Methodology

This chapter outlines the process of using CoastSat with ERDC enhancements (Vos et al., 2019) to extract shorelines at the aforementioned District test sites.

2.1 Image Pre-processing

CoastSat utilizes the Google Earth Engine to download cropped imagery from Landsat 5, Landsat 7, Landsat 8 and Sentinel-2 missions, which began collections in 1984, 1999, 2013 and 2015, respectively (Fig. 1; Vos et al. 2019). The Google Earth Engine streamlines image extraction, enables specific site selection and reduces the number of pulled spectral bands, significantly reducing download file sizes. The Landsat missions and Sentinel-2 have a revisit times of 16 and 5 days, respectively. Despite differences in satellite resolution (Fig. 1), where Landsat missions range from 30 to 80 m and Sentinel-2 collects at 10 m, a multi-step technique was employed in CoastSat to create consistent spatial resolution across all satellite images. With the imagery downloaded, a multiband raster dataset is created by fusing the high resolution sharpened panchromatic band that spans multiple spectral bands (Landsat 7 and Landsat 8) and the lower resolution from other sensors, effectively improving the spatial resolution from 30 to 15 m (Vos et al., 2019). Due to the absence of the panchromatic band in Landsat 5 and Sentinel-2, a sub-pixel down sampling technique was applied to make comparable image resolution and spatial error among all four satellite images (Vos et al., 2019). When cloud cover exceeds 10% in images they are automatically excluded.

2.2 Transect and Baseline Construction

The user is prompted to draw a reference shoreline from the first image of sufficient quality from the series. This reference line is the basis of comparison for the ML detected shorelines and used to identify “good” shorelines from the ML set. A detected shoreline point exceeding a distance of 150 m from the reference line is eliminated from the collection of detected points made for each image.

Reference baselines are constructed across each of the study sites landward of the landward-most satellite-derived shoreline. Cross-shore transects are cast perpendicular from the reference line every 1.0 m in the

alongshore as chosen by the research team. To calculate shoreline change, the intersection of each transect with each shoreline is extracted and differenced. The transect-based approach allows for the calculation of shoreline change in both the cross-shore and alongshore dimensions. A second transect collection is also produced as specified by the research team, subset from the first, with a transect every 70m. This reduces collection of transects offers adequate spatial resolution with significant performance improvements and therefore, is used in most subsequent ERDC statistical analyses. However, users can use the 1.0 m-spaced transects if needed.

2.3 Shoreline Extraction

CoastSat employs a multi-step shoreline extraction process. A manually digitized training dataset from five sites using 1500 pixels per class and accuracy of 98% was used to formulate supervised classification to categorize each pixel as 'sand', 'water', 'whitewater' or 'other' (Vos et al., 2019). Next, the Modified Normalized Difference Water Index (MNDWI) creates a grayscale image and calculates values between -1.0 and 1.0 for each pixel, where positive values represent land and negative represent water. Otsu's thresholding algorithm is used to optimize the distinction between land and water and the iso-valued contour shoreline is drawn using the Marching Squares technique (Vos et al., 2019). The shoreline extraction methodology was trained and tested at five sites with varying wave and tidal conditions and beach slopes: Narrabeen, Australia; Moruya, Australia; Tairua, New Zealand; Duck, USA and Truc Vert, France with RMSEs of 8.2 m, 11.6 m, 7.3 m, 9.0 m and 12.7 m, respectively.

The open-source CoastSat analysis requires the user to manually select images of adequate quality prior to the shoreline delineation step above (e.g., cloud presence). This process, performed for every image, could take an hour or more to evaluate a site over a typical one to two decade analysis. To reduce user workload, ERDC developed a simple machine-learning based tool to high- and poor-quality bypass this step and filter out poor images and resultant shorelines. This tool was trained from sorted image/shoreline combinations that were performed by hand previously in the project. The training set included over 1,000 usable shorelines and over 500 unusable shorelines.

The ERDC-modified version of CoastSat relies on the coordinates that define the shape of the CoastSat-determined shoreline associated with

each image. To train a k-nearest neighbors voting algorithm the shoreline length and Hausdorff distance is calculated from the already classified sites. This results in a binary classifier using the deviation of those attributes in an unclassified shoreline from a small set of user-selected high quality shorelines.

For the user this means that after a series of initial judgements provide the algorithm with sufficient information, it is capable of sorting most of the remaining shorelines independently. We have also included a check on the algorithm where after fifty independent classifications, the user is prompted to make a few more decisions to ensure that the shoreline standard is maintained despite evolution of the coastline over the analysis period. The user can QAQC and re-run the algorithm iteratively.

The shorelines produced by the CoastSat ML algorithm are a connected series of points, each of which represents a pixel that was determined to represent the interface of land and water (Vos et al., 2019). Of interest is the shoreline, but other valid interfaces may be detected as well, including swimming pools, lagoons, landscaping features, etc. Invalid interfaces may also be found including white or reflective rooftops, particularly dense clouds, etc. When the series of points is drawn together to form a linear shoreline feature these extraneous detections can cause double shorelines, offshoots, loops, and other problematic geometries. Not all of these are detected in the bad shoreline sorting above, nor is that desired, as many accurate shoreline delineations could be lost due to the presence of a static structure like a swimming pool. To reduce the quantity of data that must be discarded, a cleaning function was developed by ERDC. This function takes each set of shoreline points and measures the distance from point-to-point along the series. Clusters of points occurring more than 100m away from the longest string of neighboring points are discarded. These cleaned shorelines are saved as a shapefile at this step.

2.4 Beach Slope and Tidal Correction

CoastSat extracts the position of the wet/dry boundary, and therefore is influenced by the prevailing water level. Since the time of the image is known, a tidal correction is possible using:

$$\Delta x = \frac{z_{ref} - z_{wl}}{m} \quad (1)$$

Where in equation 1, Δx is the cross-shore horizontal shift along the shore-normal transects, Z_{ref} is reference elevation (e.g., 0.0 m above mean sea level), Z_{wl} is the local water level (tide + residuals) at the time of image acquisition (stored in metadata) and m is beach face slope. Positive ΔX infers offshore direction. Note, the tidal correction is site-specific and therefore not implemented in the standard CoastSat toolbox but added as an ERDC enhancement.

To initiate the tidal correction, ERDC added automatic selection of the closest NOAA tidal station. Since the closest station is not always satisfactory, the user can also input a choice of station. For each satellite pass a daily six-minute series is downloaded from the NOAA server.

Following this, if the user has not provided an estimate of the beach slope, the CoastSat.Slope module is used to determine the beach slope by calculating the energy inside the peak tidal frequency band for a power spectrum density of a range of hypothetical tidally-corrected time-series of shorelines (Vos et al., 2019). The minima of the integrated spectra is expected to most closely match the actual beach slope (Vos et al., 2019). The average beach slope, whether given by the user or CoastSat.Slope is then used to shift both the shoreline shapefile and the cross-shore distances table. This operation converts the previous land/water interfaces which only have a horizontal spatial orientation to a proper shoreline with an associated vertical datum as well; in this case NOAA's mean sea level. Users should be aware that the CoastSat.Slope used to shift shorelines applies only the intertidal region.

2.5 Wave Runup Correction

A correction for wave runup was explored as an addition by the team as well. The wave height closest to the time of each satellite pass is taken from a user-selected NOAA NDBC buoy. Stockdon's 2006 standard runup equation (2) is used to calculate the wave's vertical displacement from the significant wave height delivered by the buoy:

$$R_2 = 1.1\left(0.35\beta_f(H_0L_0)^{1/2} + \frac{[H_0L_0(0.563\beta_f^2 + 0.004)]^{1/2}}{2}\right) \quad (2)$$

Where H_0 is wave height, L_0 is wavelength, and β is beach slope.

These vertical dimensions from waves are used in the same manner as the tidal elevation correction above, to shift the shoreline along a given slope. The runup correction is a positive value, indicating height above the still water level, leading the runup correction to only move shorelines seaward, i.e., to negate the falsely derived, more landward shoreline resulting from wave runup.

3 Site Selection

The research team aimed to select sites that encompassed a broad range of coastal settings and environmental conditions (Fig. 2; Table 1). First, USACE districts were contacted for recommendations based on 1) areas with robust shoreline survey ground truth data, 2) areas with management challenges or beach projects (e.g., nourishments, nearshore berms) and 3) areas where traditional surveys may be difficult or costly making supplementary satellite data useful.

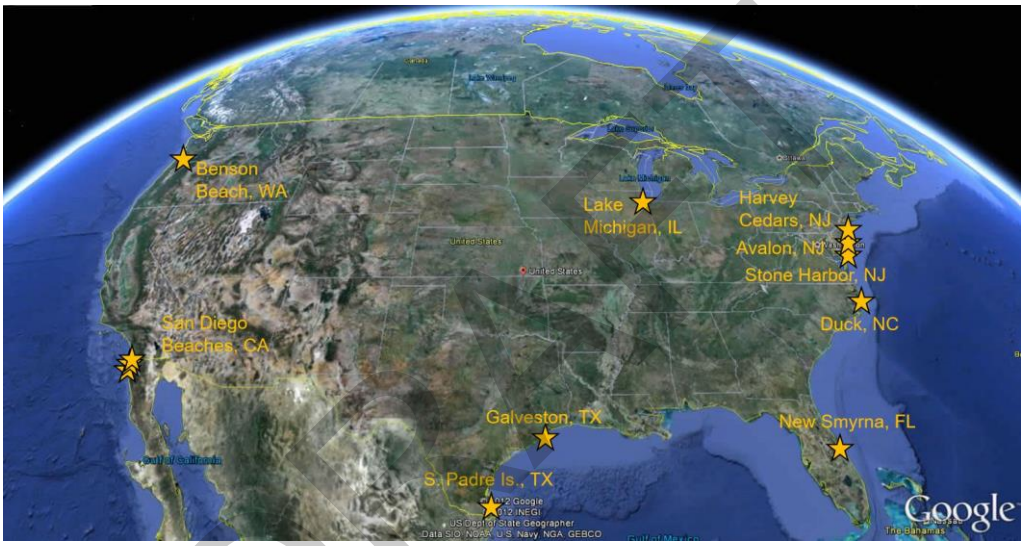

Figure 2. Test sites (stars) chosen in coordination with USACE Districts.

Table 1. Summary characteristics from test sites.

	Sig. Wave Height (m)	Avg. Wave Period (sec.)	Tidal Range (m)	Ground Truth	Mgmt. Action
Lake Michigan	n/a (wind swell)	n/a	n/a	29 UAV topo. surveys	n/a
Avalon, NJ	0.8	8.3	1.3	11 cross shore profile shorelines	Nourishments, truck hauls
Stone Harbor, NJ	0.8	8.3	1.3	11 cross shore profile shorelines	Nourishments, truck hauls
Duck, NC	1.0	7.5	1.0	407 cross shore profile shorelines	Unmanaged
New Smyrna Beach, FL	1.5	8.3	1.4	12 Mini Argus shorelines	Nearshore berm placement
Galveston, TX	0.5	5.3	0.9	5 Lidar shorelines	Nourishments, berm placements
Padre Island, TX	1.1	6.0	0.9	5 Lidar shorelines	Nourishments, groins, geotextile tubes
Imperial Beach, CA	0.9	13.0	2.2	124 DEM shorelines	One small nourishment
Cardiff, CA	1.0	13.6	2.2	124 DEM shorelines	One small nourishment, rip rap
Torrey Pines, CA	1.0	13.2	2.2	124 DEM shorelines	One small nourishment
Benson Beach, WA	2.2	11.0	3.1	84 DEM shorelines	n/a
Harvey Cedars, NJ	0.9	6.4	1.3	9 cross shore profile shorelines	Nourishments, Nearshore berm

3.1 Lake Michigan, Illinois

In the interest of testing a lacustrine shoreline, the research team coordinated with the Chicago District and Michigan State University (Dr. Ethan Theuerkauf; Department of Geography, Environment, and Spatial Sciences) to obtain ground truthed shoreline data along Lake Michigan. The testing site is located along the southwestern shoreline of Lake Michigan in northeastern Illinois and is part of the Illinois Beach State Park. The shoreline is composed of sand as a ridge and swale complex (Theuerkauf et al., 2019). An outwash deposit was reworked around 4,500 years BP into a strandplain beach and has been characterized by erosion in the northern portion (this site) and accretion to the south through predominant southerly alongshore transport of eroded sediment. Sensitive to fluctuating lake levels (Fig. 3), the beach ridges have experienced cyclic destruction and formation where low lake levels promote growth and high levels trigger erosion (Fraser et al., 1990). In the late 1800s, jetties and other stabilization structures were constructed to the south to slow the net southerly migration of the beach ridge complex (Chrzastowski et al., 1996). After low water levels in the early 2000s, the lake rose rapidly at over 0.5 m over six months in 2014 (Fig. 3, red circle), resulting in accelerated erosion and habitat loss. The specific testing site is characterized by a narrow ~10 m beach and a small foredune (<1.5 m) which makes it susceptible to overwash (Fig. 4).

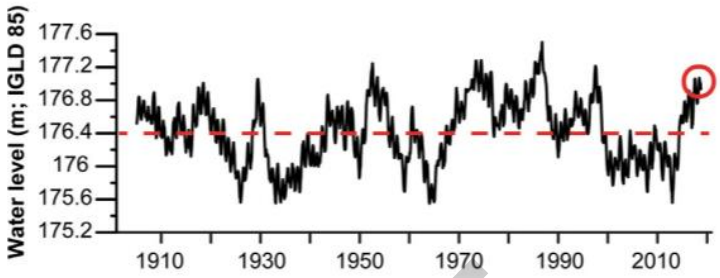

Figure 3. Lake Michigan water level fluctuations since 1900 from Theuerkauf et al. 2019.

Over the six km testing site, 29 unmanned aerial vehicle (UAV) surveys were collected by the Theuerkauf group between July 2018 and January 2021, with the goal to evaluate the hydrodynamic conditions responsible for rapid erosion, specifically whether water levels alone are the primary control or whether certain wave conditions are also a significant factor. A DJI Phantom 4 Pro quadcopter was used to collect high resolution imagery (20 megapixel) with 80% overlap and Agisoft Metashape was used for structure-from-motion photogrammetry. Ten to fifteen ground control points were evenly spaced throughout the site and were surveyed using a Trimble GEO 7X GPS system and RMS errors of the constructed elevation surface were less than 5 cm. Shorelines were digitized from these robust elevation surfaces based on the land/water interface from the edges of the point clouds and ortho imagery.

Figure 4. UAV imagery collected from the beginning and end of the study used for ground truth shoreline data. Note the strong erosion over the time interval and loss of the road (orange arrow).

3.2 Avalon and Stone Harbor, New Jersey

Figure 5. Oblique aerial photograph looking southwest of the Avalon, NJ study site.

Avalon and Stone Harbor New Jersey are located on a barrier island on the Atlantic Ocean coast of New Jersey, bound by Townsends Inlet to the North and Hereford Inlet to the south (Fig. 5). During the Quaternary Period, sea level changes caused the spreading of sand and gravel deposits that have been reworked through time. The Cape May formation in particular was deposited along valley bottoms and estuarine/marine zones to form the shoreline during the last interglacial when sea level was ~10 m higher than present. The average wave height in the region is 0.8 m with a wave period of 8.3 seconds (Thompson, 1977). The tides are semi-diurnal with a range of 1.3 m (Dally and Osiecki, 2018).

Subject to major flooding and erosion during storms, a feasibility study for mitigation over a 15-mile stretch began in 1992. The first coastal storm risk management (CSRM) project was constructed in 2002 by USACE at each town. While a three-year renourishment interval was authorized, there was not sufficient federal funding for renourishment until 2016. As a federal alternative, the Borough of Avalon, sometimes in partnership with the NJ Department of Environmental Protection, placed 2.4 MCY of sand between 2005 and 2016 along the erosional hotspot of Avalon (Fig. 5). In addition, USACE added truck hauls (2009) and emergency beachfills

(2011 and 2013) totaling 961,000 CY. The last nourishment of 1,636,685 CY was conducted in 2017.

Beginning in 2002, 56 profile lines were surveyed from the dune through the depth of closure using a combination of GPS, ATV and boat data for a nourishment feasibility study. The ground truth for satellite shoreline comparison consists of 11 shorelines collected between 2002 and 2019 which were generated using the original 56 beach profiles from 2002 with the addition of three profile lines.

3.3 Duck, NC

Duck is located on a narrow and long barrier island on the Atlantic coastline in the northern Outer Banks in North Carolina (Fig. 6). Tides are semi-diurnal with a mean range of ~1 m and mean significant wave height is 1.0 ± 0.6 m (Lee et al., 1998). Duck is prone to high wave energy in the winter from nor'easters, or extratropical systems, and hurricanes in the summer and fall months. Dominant longshore transport is from north to south and is largely storm driven (Dolan et al., 1988). An artificial dune was constructed in the 1930s and 1940s to protect the roadway (Birkemeier et al., 1984).

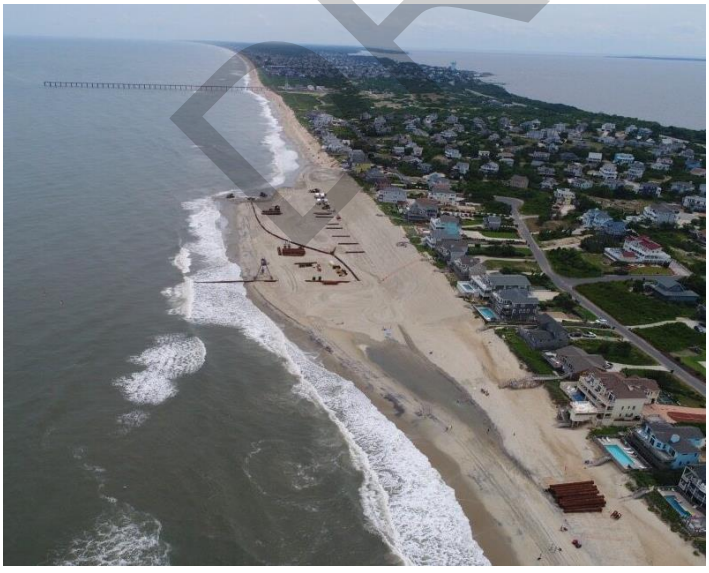

Figure 6. Duck, NC 2017 beach nourishment. USACE Field Research Facility Research Pier is visible in top of frame.

The U.S. Army Corps of Engineers Field Research Facility (FRF) was constructed in Duck in the late 1970s and has since been a world-renowned coastal observation facility (Fig. 6). The FRF has the unique ability to collect data within the challenging surf zone using amphibious vessels and custom instrumentation. The monthly subaqueous and subaerial survey of the property (1 km long) has been a staple of the FRF observational record since the early 1980s (Birkemeieir et al ., 1984).

Profile data from these frequent monthly surveys is highly accurate (~3 cm error; Forte et al., 2017) and was used for comparison with satellite-derived shorelines. Duck was nourished for the first time in 2017 (1.0 MCY) and the project stopped at the northern property boundary of the FRF, allowing for an opportunity to monitor project equilibration and longshore diffusion of the added sand.

3.4 New Smyrna Beach, FL

New Smyrna Beach is located on a barrier island on the Atlantic Coast in central Florida (Fig. 7). Ponce de Leon Inlet is located just north of the town and experiences problematic, chronic shoaling, requiring regular dredging. This region of central Florida is characterized predominantly of Holocene barrier deposits and dominant longshore transport is southerly with a seasonal reversal to the north in the summer (Stapor and May, 1983).

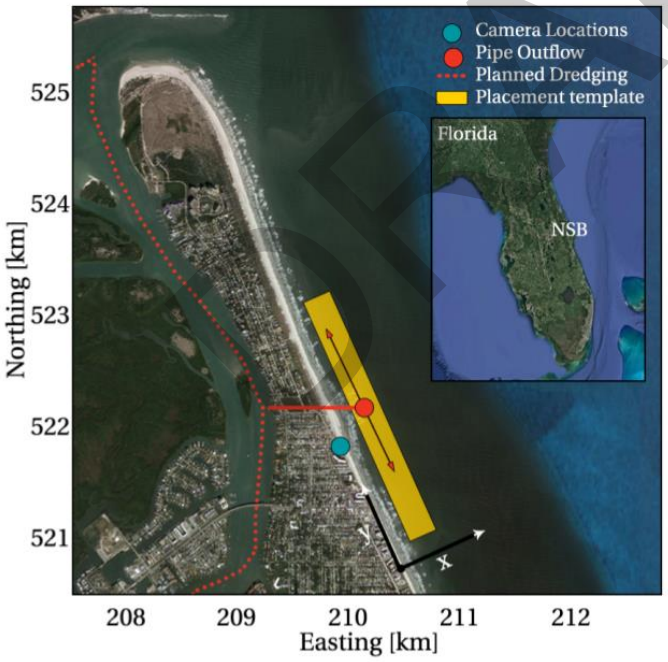

Figure 7. New Smyrna Beach and location of dredge and nourishment activities. Adapted from Bruder et al. (2019a).

New Smyrna Beach has historically been impacted by hurricanes and nor'easters, causing extensive shoreline erosion. From August 2018 through March 2019, 350,000 m^3 of sediment was dredged from Ponce De Leon Inlet to reduce shoaling and was placed via pipeline in the nearshore of New Smyrna Beach at approximately 4 m water depth (Fig. 7; Onnink, 2020). This nearshore berm nourishment was monitored hourly by CHL researchers using a mini-Argus camera system mounted on a high-rise building consisting of four cameras collecting snapshot, timelapse, variance, brightest and darkest imagery from August 2018 to September 2019 (Fig. 8) (Bruder et al., 2019). Specifically, shorelines were manually digitized using the georectified timex imagery following methods outlined

in Bruder et al. (2019). The manual digitization approach is estimated to have a precision on the order of 10 m (Onnink, 2020). Timex imagery is time-averaged during the collection time (10 minutes) and has been successfully used in the past for extracting shoreline positions (Lippmann and Holman, 1989; Holman et al., 1993). During the deployment, significant wave height was 1.5 m, mean wave period was 8.3 seconds and the maximum tidal range was 1.4 m.

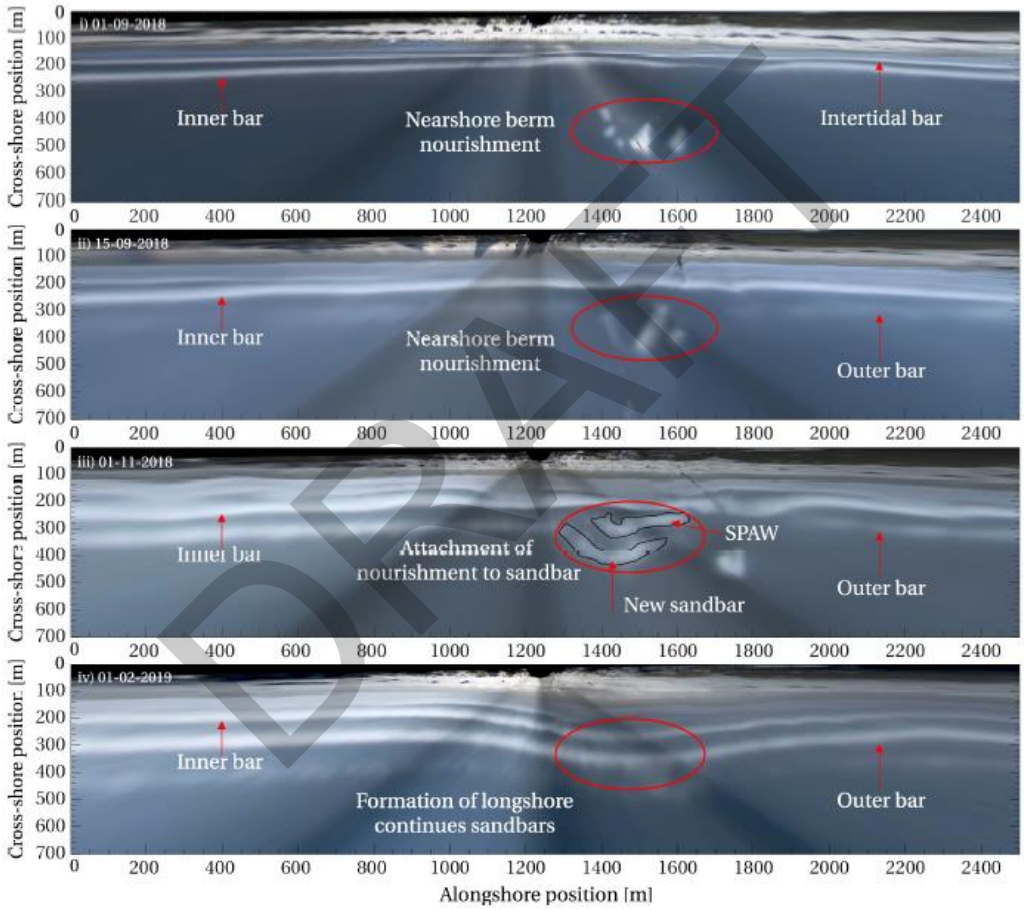

Figure 8. From Onnink (2020), Timex imagery from the CODS mini-argus deployment from (top to bottom) Sept. 1, 2018, Sept. 15, 2018, Nov. 1, 2018, Feb. 2, 2019 capturing various stages of evolution following the nearshore berm placement. "SPAW" represents shoreward propagating accretionary wave.

3.5 Galveston and Padre Island, TX

An extensive study by the Texas Bureau of Economic Geology (Paine et al., 2021) found significant net coastal retreat on Galveston and Padre Islands, TX, both tourist destinations that represent valuable habitat, industrial infrastructure and economic resources to the state. Because of the shoreline behavior and management challenges, the Galveston District (SWG) recommended the sites for satellite testing.

The Texas Coast is characterized by complex geologic history. The shoreline position is a function of multiple related coastal processes including sea-level change, land subsidence, sediment influx, littoral drift and storm impacts/recovery (Paine et al., 2021). The coastline includes the Holocene geomorphic features of barrier islands, strandplains, fluvial and deltaic headlands and chenier plains (Aronow et al., 1982; Brown, Brewton, and McGowen, 1975; LeBlanc and Hodgson, 1959). Three major rivers impact hydrodynamics and sediment supply along the coast (Brazos, Colorado, and Rio Grande), although construction of dams for flood control and water supply have reduced sediment loads. During the Holocene transgression, Galveston Bay formed landward of the barrier islands as Pleistocene river valleys were submerged. A convergence zone occurs at Padre Island where currents generated from southeasterly winds meet the Rio Grande deltaic headland to the south and the Brazos-Colorado headland to the northeast. Relative sea level rise is a major factor influencing coastal processes along the Texas Coast, and the Galveston Pier 21 has the longest period of water level record showing a long-term rate of sea-level rise of 6.55 mm/yr (between 1904 and 2019). The Texas Coast has been impacted by a plethora of tropical storms through time, notably Hurricane Ike (2008) and Hurricane Harvey (2017).

According to district records, a total of 20 beach projects have been conducted between 2000 and 2021 for Galveston and Padre Island beaches. Of these projects, five included placement of less than 6,000 CY. Three projects were related to dune construction and the placement of geotextile tubes (2000, 2007, and 2009). The largest project was conducted in 2017 involving one MCY yards of nourishment throughout the Galveston groin field. At South Padre Island, a total of 15 beach projects were completed between 2000 and 2021. Of those, seven were berm placements and eight were nourishments. Placement volume ranged from 220,000 CY to 500,000 CY. The eastern portion of the Galveston

shoreline includes a series of groins for sediment capture, which has created distinct shoreline configuration (Fig. 9).

Figure 9. Oblique aerial image of Galveston Island. Note the numerous jetties.

Shoreline positions were extracted from airborne lidar topographic datasets from 2010, 2011, 2012, 2016 and 2019 (Paine et al., 2021). Shorelines were delineated at an elevation contour from the 1-m resolution DEM that approximate the wet beach/dry beach boundary consistent with historical use in shoreline studies. This wet/dry interface was checked by superimposing the lidar data on georectified National Agricultural Imagery Program aerial imagery (Paine et al., 2021). Lidar data was georeferenced and compared to GPS-derived ground control points and calibration targets. All lidar surveys were flown in late winter or spring, other than the 2016 survey that was conducted in fall.

3.6 San Diego Beaches, CA

In coordination with USACE, Scripps Institute of Oceanography has collected long-term, high resolution subaerial and subaqueous coastal monitoring datasets. In 2019, Ludka et al. published a summary paper and released a dataset covering three reaches of San Diego coastline (Torrey Pines, Cardiff and Solana). The data span between eight to 16 years (2001 – 2016) and spatial extents vary from 4.2 to 7.9 km in the alongshore. For this work, monthly to quarterly topographic surveys at 100 m spaced cross-shore transects were used to extract the shoreline position for comparison to satellite data.

This region of coastline is hydrodynamically and geologically complex (Ludka et al. 2019). Rocky headlands, nearshore submarine canyons and offshore shoals contribute to alongshore wave variability, in addition to the nearby Channel Islands that create shadowing and refraction effects

over variable shelf bathymetry. Generally, the winter season produces the most energetic waves from the North Pacific and promotes southerly longshore sediment transport and the milder summer South Pacific swell causes shoreward and northerly transport. Seacliffs back much of the coastline and are composed of a bottom unit of lithified Eocene and Miocene mudstone, shale, sandstone, and siltstone, and a top unit consisting of unlithifed Pleistocene terrace deposits. Cobbles are intermittently exposed along the beaches, most often when beach sands are eroded (Ludka et al., 2019).

The Torrey Pines stretch contains reef, a lagoon mouth and the landward tip of the Scripps Submarine Canyon. In 2001, monitoring was initiated to capture the evolution of a subaerial beach nourishment project constructed in 2002 to protect an adjacent major roadway. Data showed rapid (monthly) transport of the nourished sediment to an offshore bar followed by the partial return of the sediment through onshore transport in the summer. Much of this region is characterized by cobble (Fig. 10).

The majority of Cardiff and Solana also contain reef and have lagoon mouths at the northern and southern boundaries. While Solana is backed by cliffs, Cardiff contains rip rap to stabilize the roadway and parking lots that are often flooded (Fig. 10). In 2012, both beaches were nourished and observations showed minimal loss of the sediment from the subaerial beach over the course of a few years.

Imperial Beach contains the Tijuana River Mouth and offshore cobble shoal to the south, along with a recreational pier and two short jetties (100 – 150 m) to the north. Some homes are protected by rip rap and small dunes (Fig. 10). This beach was also nourished in 2012 and had similar success to Cardiff and Solana, yet eventually the nourished material was transported to the river mouth causing problematic clogging and consequent degradation of water quality in the estuary (Ludka et al., 2019).

Figure 10. Low tide photos of Cardiff, Torrey and Imperial Beaches from Ludka et al. 2019.

The subaerial survey data were collected with an ATV (shocks removed, constant tire pressure) at low tide in combination with a push dolly, both outfitted with high precision Global Navigaton Satellite System (GNSS). Subaqueous data was acquired with a personal watercraft outfitted with a 192 kHz acoustic sonar, a sea surface thermistor for speed of sound calculations and GNSS antenna. The combination of the three methods ensured continuous profile overlap across the surf zone (Ludka et al., 2019).

3.7 Benson Beach, WA

The high wave energy coupled with large sediment-laden river systems in Washington State creates many dynamic coastlines. With input from several district engineers, Benson Beach at the mouth of the Columbia River (Fig. 11) was selected for satellite validation, primarily due to dense data availability over the past two decades and history of challenges in managing the stretch of coast. Beginning in 1996, the Washington Department of Ecology in conjunction with the U.S. Geological Survey and Oregon State University spearheaded a comprehensive coastal monitoring program for the state, generating frequent high resolution morphology datasets. The primary goals of the study were to “improve scientific understanding of coastal morphodynamics and sedimentary processes, to determine natural and anthropogenic influences of the littoral system, and to provide information and predictions of coastal behavior at temporal scales of decades and spatial scales of tens of kilometers (Kaminsky et al., 1997; Gelfenbaum et al., 1997; Kaminsky et al., 1999; Ruggiero et al., 2005). In addition, these data enable the testing and development of hydrodynamic and sediment transport models in the region.

The Columbia River Littoral Cell (CRLC) extends between Tillamook Head, OR and Point Greenville, WA. Two large estuaries, Willapa Bay and Grays Harbor, lie to the north. A relatively slow rate of eustatic sea-level rise ~6,000 years ago caused the formation of modern barrier islands and strandplains as the shelf and estuary filled (Kaminsky et al., 2010). Beaches began to prograde about 4,500 years ago. Situated along an active tectonic margin, earthquakes have caused coastal subsidence and shoreline retreat over an estimated 500-year recurrence interval (Kaminsky et al., 2010). Yet despite the seismic influence, the coastlines have been net progradational due primarily to high sediment load delivered from the Columbia River that is redistributed by the strong wave climate. The Pacific Northwest is notorious for a severe wave climate, generally producing ~10 m high and (Hs) long period (13 seconds) winter storm waves at least once annually. The combination of high wave climate and fine-grained sands gives the CRLC a morphodynamic classification of 'modally dissipative' (Wright and Short, 1983; Ruggiero et al., 2005), dominated by low-frequency infragravity energy in the nearshore zone. Tides are mixed semi-diurnal ranging from 2 to 4 m (mesotidal). Driven by winter wave/wind energy, the net sediment transport is to the north (Kaminsky et al., 2010).

Figure 11. Benson Beach with Columbia River jetty in the background. Notice the narrow, steep beach and storm-deposited debris.

The comprehensive monitoring program contains the primary components of cross-shore topographic beach profiles, 3-D topographic beach surface maps and nearshore bathymetry. For this study, researchers obtained 84 beach surface maps collected roughly bi-annually to quarterly from 1997 to 2019. The site was nourished in 2002 (43,000 CY). Data were collected with an all-terrain vehicle (ATV) equipped with survey grade D-GPS receiver, GPS antenna, Radio modem, radio antenna, data logger, and cabling to the RTK backpack that is also used for typical beach profile surveys. Differential corrections were provided by a geodetically fixed RTK GPS base station. Data points were densely spaced in the alongshore to resolve small scale features (e.g. cusps, berms) and cross-shore transect spacing was on the order of ~10 m, although drivers used discretion to determine the most optimal path for capturing the variability of features. The ATV data collection spanned from the foredune toe to the swash zone. Data were manually checked for quality, then Matlab scripts were used by Washington Department of Ecology to map non-uniformly spaced raw data onto a 2-D gridded surface through weighted linear interpolation. Comparisons with robust beach profile surveys show that the vertical RMS error of the ATV interpolated beach surface is typically less than 5 cm in the horizontal dimension and 10 cm in the vertical dimension.

3.8 Harvey Cedars, NJ

Harvey Cedars is located on a barrier island on the Atlantic Coast in central New Jersey. The beach is roughly 3 km long and faces east/southeast. Average wave heights in the region are 0.9 m and average wave period is 6.4 s (Cialone and Thompson, 2000). The tides are semi-diurnal with a range of 1.3 m (Dally and Osiecki, 2018).

Identified as an erosional hotspot, Federal Coastal Storm Risk Management (CSRM) has constructed groins and the first project in 2010. Since this project, three renourishments have followed including emergency repair from the impacts of Hurricane Sandy. The last, most recent management project at Harvey Cedars was the emplacement of a nearshore berm. In the summer of 2021, 83,300 m^3 was dredged from Barnegat Inlet and placed in the nearshore (- 2.75 m NAVD88 depth) of Harvey Cedars by the Philadelphia District (NAP). WRDA's Sect. 1122 program supports experimental beneficial use projects such as this effort. Nine topographic and bathymetric surveys conducted during this project serves as ground truth for satellite comparisons. RTK-GPS and single

beam transects were spaced every 75 m (26 total) and combined to create DEMs. Work to analyze the evolution of the placement is ongoing using in situ hydrodynamic sensors and satellite-derived shorelines (McGill et al., 2022; accepted).

4 Instantaneous Shoreline Comparisons

A primary goal of this effort was to quantify the accuracy of CoastSat using ground truth data from test sites across the nation. Overall, across all sites the mean horizontal difference from the ground truth shorelines was 14.1 m (Fig. 12). However, Fig. 12 highlights the variability in the skill where mean horizontal differences from ground truth ranged from 4.8 m to 32.0 m. Interestingly, individual sites within the same study area also performed at varying accuracy. For example, mean horizontal differences at adjacent sites on South Padre Island ranged from 4.79 m to 21.31 m(Fig. 12). The Lake Michigan region also exhibited variabilty in accuracy performance with a range of 9.09 m to 17.84 m in mean horizonal difference. This regional variabilty in accuracy may be due to several potential factors including image coregistration differences across the region.

The results of this work use output from CoastSat v1. During this effort, our research team and the CoastSat creator (Vos, 2022, per. communication) each discovered co-registration issues related to Google Earth Imagery ingestion that was essentially rounding area of interest polygons and resulted in offsets among satellite missions. This issue has since been partially corrected in CoastSat v2.

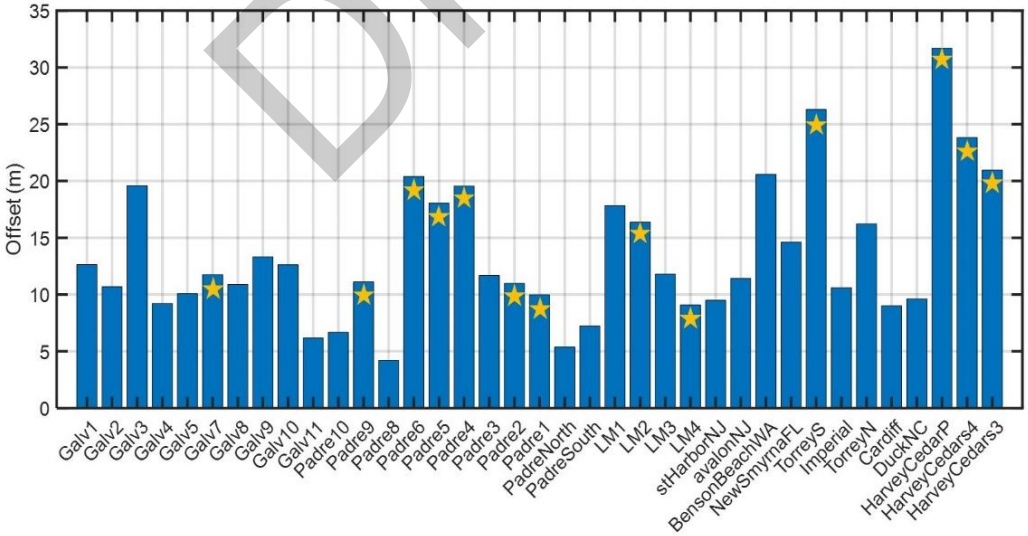

Figure 12. Summary of mean horizontal difference (offset) of satellite-derived shorelines compared to ground truth surveys across test sites. Orange stars indicate sites with apparent Google Earth Engine imagery issue that will be omitted from subsequent analysis.

This mission offset can be visualized in Fig. 13. Within geographic regions some 3 km sites showed good alignment between satellite missions, while others showed mission offsets, some of which were significant (~20-40 m). An example of this is shown in Fig 13a, b from South Padre Island where Padre3 (panel a) shows no apparent issue and adjacent Padre4 (panel b) shows an offset between Sentinel-2 (blue) and Landsat-8 (red). This is likely a driving factor in differences in instantaneous shoreline accuracy at those sites (mean horizontal differences at Padre3 = 12 m; Padre4 = 19 m). In the case of Padre 4, the Sentinel-2 (blue) data seem to align with the ground-truth, whereas Landsat-8 data are offset as a separate population. Panel c of Fig. 13 shows a similar issue at Harvey Cedars, also with poor satellite shoreline accuracy (30 m mean horizontal difference). Overall, 13 out of 37 sites displayed this issue. Vos (personal communication, 2022) was able to determine the mission offset issue stems from Google Earth Engine (GEE) imagery download. It is hypothesized that when the CoastSat user draws an AOI polygon for a site, the GEE rounds the pixel coordinates, and returns a slightly shifted image, resulting in offsets at some sites. It is unclear why this happens for some sites and not for others. This has been addressed for LandSat-8 in CoastSat 2.0 through new imagery download and preprocess functions that provide better alignment between panchromatic and multispectral bands. The CoastSat 2.0 update does not yet include the shift fix for Sentinel-2. Coloring shoreline positions through time by satellite mission should provide the user a quick assessment tool to determine if this offset is a problem for their site of interest.

Sites where this problem is evident have been starred in Fig. 12. Since this report focuses on the performance of the CoastSat algorithm, and the issue is associated with Google Earth Engine, we have omitted results from the problematic sites from subsequent analysis. When these sites are not included, the overall mean horizontal difference between satellite-derived shorelines and ground-truth shorelines is reduced to 11.32 m.

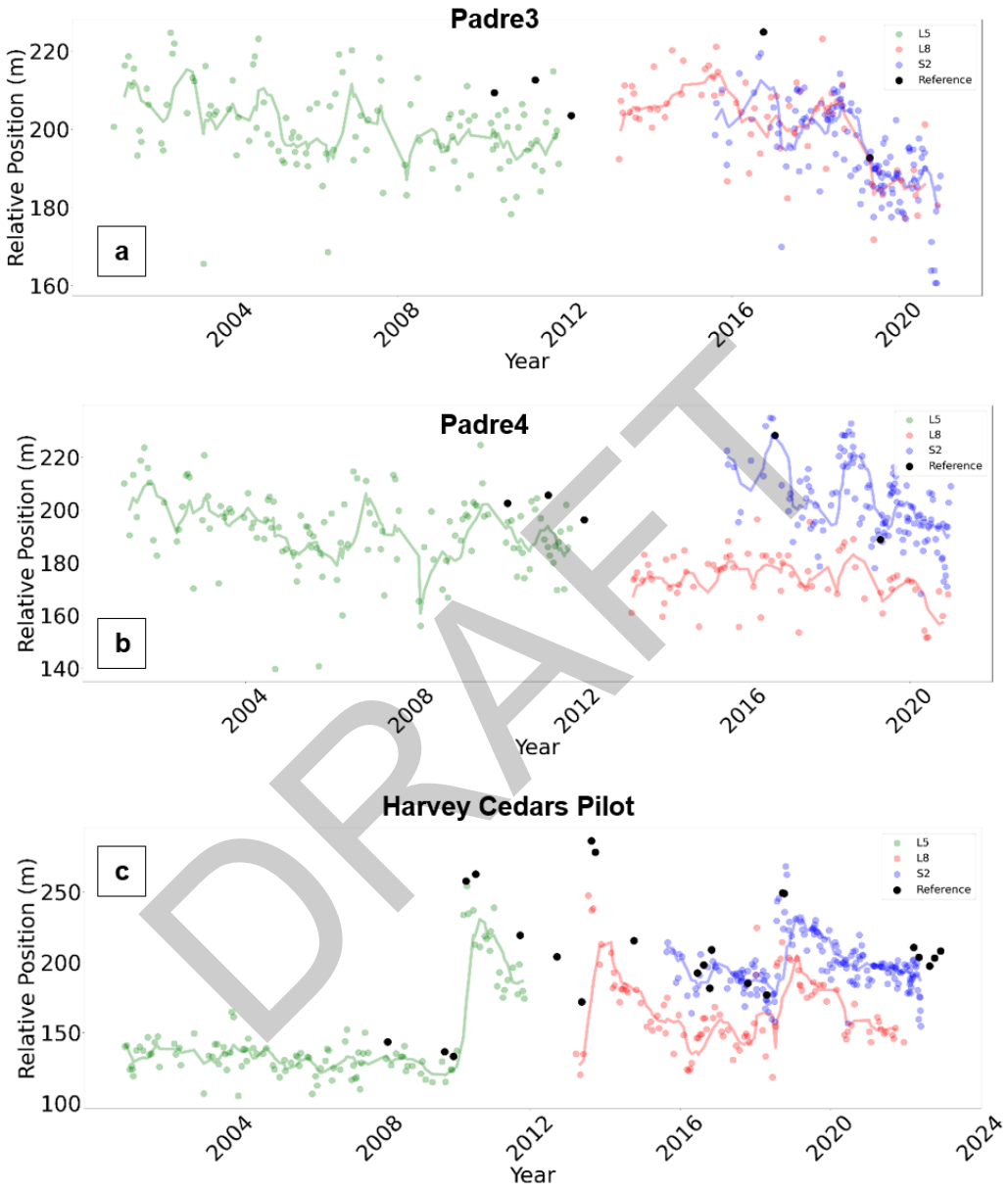

Figure 13. Shoreline positions through time for Padre3 (a), Padre4 (b) and Harvey Cedars Pilot (c). Points are colored based on satellite mission. Notice good alignment across missions in panel a, and misalignment of Landsat-8 (red) and Sentinel-2 (blue) in panels b and c.

In terms of bias, results show a mean direction of -3.51 m (SD = 12.57 m), indicating a slight onshore bias for the satellite-derived shorelines when compared to survey-derived shorelines. Specifically, 37.5% of sites were biased towards the offshore and 62.5% of sites were biased in the onshore direction.

At Duck, we found a shoreline position RMSE of 8.50 m, which is consistent with Vos et al. (2019) who reported a RMSE of 9.0 m. It should be noted that Vos et al. (2019) conducted comparisons at a single transect and our comparisons extended 1-2 km in the alongshore, depending on the length of the FRF survey at specific times. Fig 14 provides visual examples of low and high shoreline position accuracy time intervals at Duck. An example of the consistent landward shoreline bias at Duck is evident in Fig 14 (right panel) where a mean horizontal difference from ground truth in shoreline position of 21.1 m is visible.

Figure 14 Examples of high and low accuracy satellite shorelines relative to ground truth surveys at Duck. Note the crossing shorelines in the left panel.

4.1 Satellite Mission Comparisons

Since CoastSat ingests Landsat and Sentinel imagery, we examined each satellite mission separately for accuracy and bias for all sites. Each satellite mission shows a different bias where negative values indicate shoreward direction bias and positive values reflect seaward bias (L5 = -6.93 m, L8 = -1.21 m, S2 = 1.90 m)(Fig. 15). The mean horizontal difference from the reference shorelines was L5 = 10.52m, L8 = 10.57m, S2 = 8.86m (Fig. 15). With each generation of satellite, bias and mean horizontal difference decrease. Landsat 5 and 8 have a mean horizontal difference that is 53 and 58% lower than the native short-wave infrared (SWIR) resolution of 30 m, respectively. The mean horizontal difference for Sentinel 2 is 41% lower than its SWIR resolution of 20m.

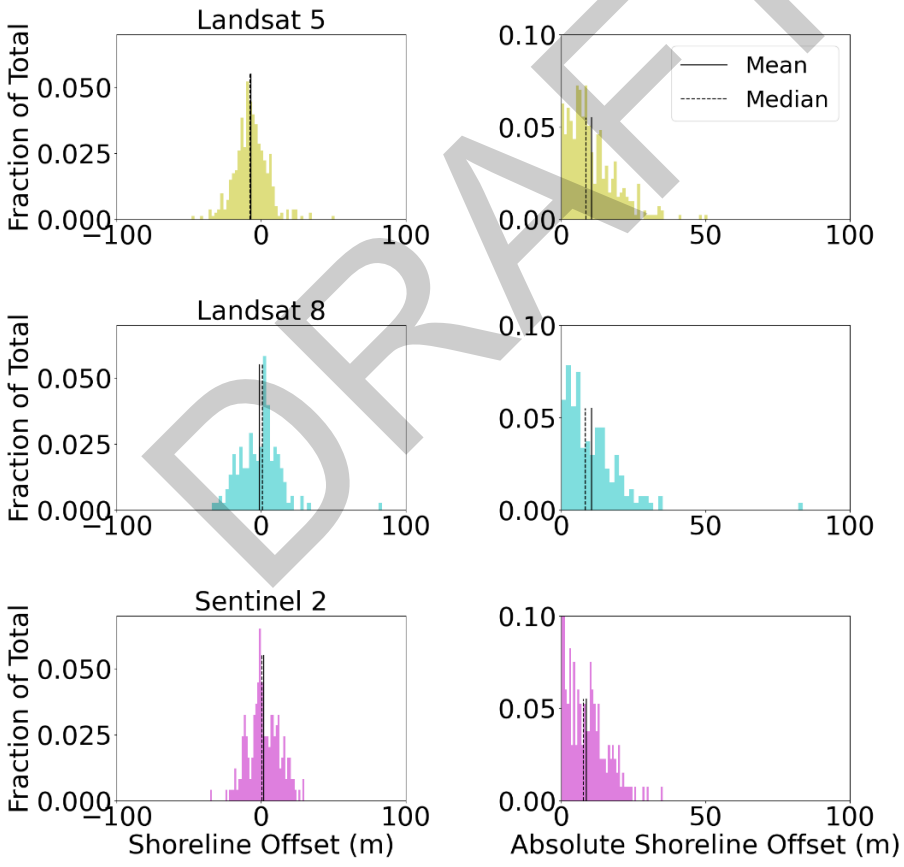

Figure 15. Mean horizontal differences in satellite shorelines from ground truth for different satellite missions. Negative values represent the landward direction and positive values are seaward relative to ground truth surveys. The absolute shoreline offset panels disregard the directional biases.

4.2 Image Co-registration

One of the major challenges of using satellite images to track environmental conditions through time is the imprecise georeferencing accuracy for the images themselves in addition to the differences in georeferencing accuracies when utilizing multi-sensor datasets. While Landsat 7 has a reported image registration accuracy (LE90) of 12.0 m (Storey et al. 2014) and Sentinel-2 has a reported image registration accuracy of 12.5 m (Trémas et al. 2015), Storey and others (2016) estimate that the sensor data can be misaligned by 38 m. One of the challenges involved in co-registering the images is the quantity and spatial extent of images used in remote sensing applications such as this, causing it to be temporally and computationally expensive (Scheffler et al. 2017).

There are multiple strategies when aligning imagery which can be simplified into two main groups – intensity-based and feature-based. Intensity-based techniques rely on similar patterns of grey values in the image, while feature-based processes look for specific identifiable objects. Feature-based processes tend to be less computationally and temporally expensive, but require features to be evenly distributed throughout the image which can be difficult to rely on in coastal environments. Because of this, applying intensity-based processes to the imagery was investigated in this study. Intensity-based processes are more computationally expensive, but do not rely on distinguishable features and can achieve sub-pixel shifts (Scheffler et al. 2017, Priyanka et al. 2020).

Two co-registration tools were investigated using satellite images of Wrightsville Beach, NC; AROSICS and the Arcpy georeferencing tool. Wrightsville Beach was not included in the statistics of the report, but it is an area of interest as it lies just east of the Wilmington District. AROSICS, which stands for Automated and Robust Open-Source Image Co-Registration Software for Multi-Sensor Satellite Data, is an intensity-based registration technique using phase correlation. While this tool is open-source and python-based, multiple problems arose when trying to integrate this tool into the CoastSat workflow. It is anticipated that the imagery format, as downloaded from GEE and different per mission, caused difficulties when using AROSICS to co-register the whole dataset together. Instead, images could only be registered to its same missions' baseline. In theory, this would still perpetuate the known offsets between missions (38 m). There are two functions in the AROSICS package, COREG and COREG_LOCAL. COREG applies a global X/Y translational

shift to the image, whereas COREG_LOCAL creates a dense grid of tie points, filters the tie points for false positives, and uses the valid tie points to fine-tune the parameters in an affine transformation. A cubic resampling technique is applied to finally warp the image. Because spatial offsets between images are highly varying, COREG_LOCAL was applied to the imagery. This process was very computationally expensive and would require many hours to complete the whole Sentinnel-2 dataset for Wrightsville Beach (91 images). Additionally, the subsequent efforts to map the shoreline from the co-registered image using CoastSat were unsuccessful. We believe this is because the SWIR band was not co-registered along with the RGB bands. This would cause the supervised classification to resemble the co-registered image, but the MNDWI would have artifacts resembling the original image. This prompted investigation of other methods to co-register the dataset.

Arcpy was a much simpler tool to integrate into the workflow and was much faster, on the scale of minutes (about 0.5 seconds an image for a total of 45.5 seconds for the 91 images) versus hours to co-register all of the Sentinnel-2 images in the test site to a base image with low initial registration error as evident in the metadata. Arcpy generates tie points (Fig. 16) from an intensity-based approach and then fits a first-order polynomial transform to warp the image (Fig. 17). The difference between the raw and co-registered, an example of which is shown in Fig. 17C, was typically subtle and can be detected mostly in shifts of bright infrastructure. Because Sentinel-2 has worse georeferencing and to save time for the end user, this process was applied to just the Sentinel 2 images from the test site to investigate the impact it had on the shoreline positions mapped using the CoastSat algorithm (Fig. 18).

Figure 16. Wrightsville Beach image with tie points shown in red and green B's.

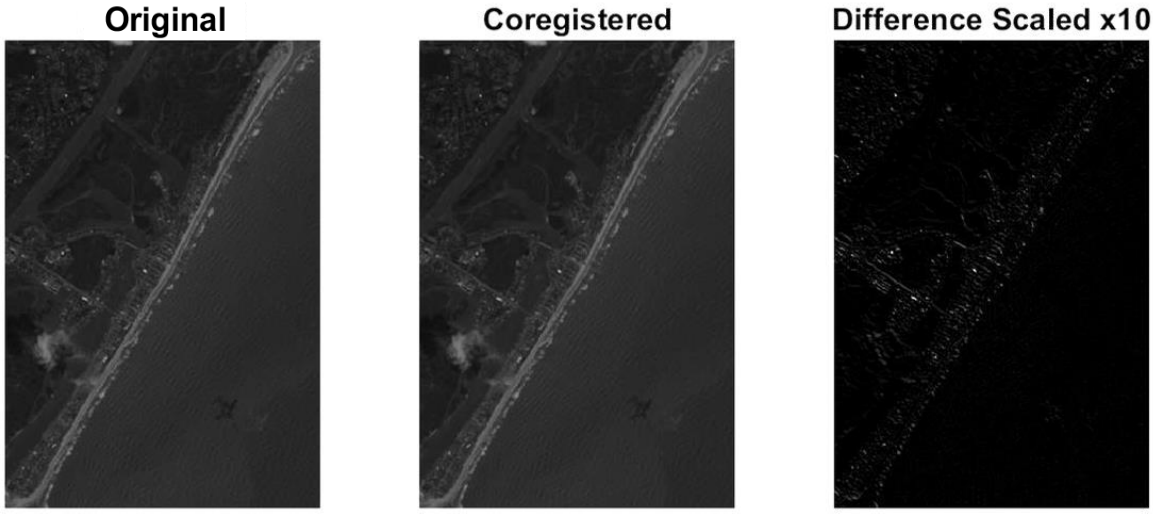

Figure 17. A) unregistered image of Wrightsville Beach B) a co-registered image of Wrightsville Beach using ArcPy C) the difference in the two images scaled to a factor of 10.

As shown in Figure 18, in the northern portion of transect 1140, the mean position was shifted landward (down) from the raw shorelines (dark blue) to the co-registered shorelines (light purple).The detrended standard deviation for transect 1140, a proxy for noisiness, was reduced from 9.90 m to 8.99 m after co-registration. In addition, the shoreline change rate changed from -4.6 meters per year to -4.4 meters per year. The southern transect (transect 1030) shows a similar change in mean shoreline position and noisiness. The detrended standard deviation for transect 1030 was reduced from 12.17 m to 9.99 m after co-registration. The shoreline change rate at transect 1030 changed from -1.88 meters per year to -0.56 meters per year. As shown in these two transects along Wrightsville Beach, if appropriate tie points are picked, the spread of shorelines could be reduced, thus decreasing the noise of the satellite-derived shoreline positions and potentially leading to lower RMSE and a better depiction of historical shoreline movement.

After seeing a reduced spread of shorelines, the same process was applied to the Duck Sentinel-2 images. Unlike Wrightsville Beach, Duck has an ample amount of ground-truth data that we can compare to our co-registered shorelines quantitatively. Using the ArcPy newly co-registered S2 images (n=548), the associated mean horizontal difference in satellite-derived shorelines compared to ground truth only improved by 6 cm. This minimal improvement in accuracy suggests mission to mission (e.g. Landsat-8 vs. Sentinel-2) co-registration may be more critical than intra-mission, though more tests are needed at additional sites with good ground-truth data. Furthermore, if the seed or base image used for co-

registration has high georeferencing error, matching other images to the base image may even increase overall errors. Thus, it is critical to ensure your baseline image has high-accuracy. While it is not practical within the current AROSICS or ArcPy framework, a potential improvement may be using a high-resolution base image to register other imagery with, such as UAV image or higher resolution satellite image (e.g. PlanetScope).

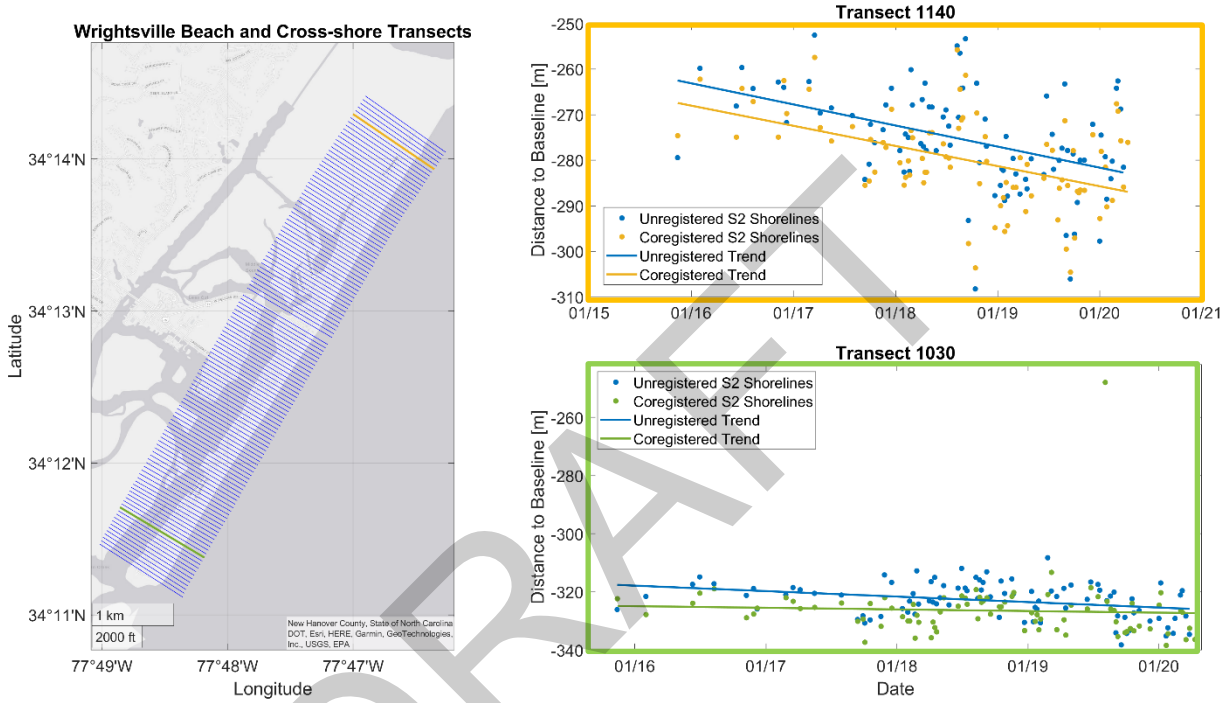

Figure 18. Left) Wrightsville Beach with the cross-shore transects used to analyze shoreline change; Top Right) Shoreline positions from unregistered and co-registered imagery at transect 1140 and their respective trends; Bottom right) Shoreline positions from unregistered and co-registered imagery at transect 1030 and their respective trends.

4.3 CoastSat-generated Slopes

To correct visually identified shorelines to a consistent datum-based shoreline, the tide level and slope are used in CoastSat. Beach face slope is a fundamental parameter for coastal research related to shoreline change, runup and flooding, yet it often varies through time and is difficult to quantify without conventional field observations. Vos et al. (2020) added the automated capability to extract slopes from historic satellite imagery through the CoastSat.Slope toolbox. Vos et al. (2020) found good agreement (R2 = 0.93) with the approach compared to field observations at eight sites across the globe.

We tested the CoastSat.Slope function at the district test sites and compared the output to field survey slopes, where robust slope data was available. It is important to note that even field-based surveys are only capturing slopes at one point in time and, in reality, slopes are likely time varying. Fig. 19 shows the comparison of CoastSat-derived vs. user input slopes (i.e., measured) with poor agreement (R^2 = 0.24) for the test sites.

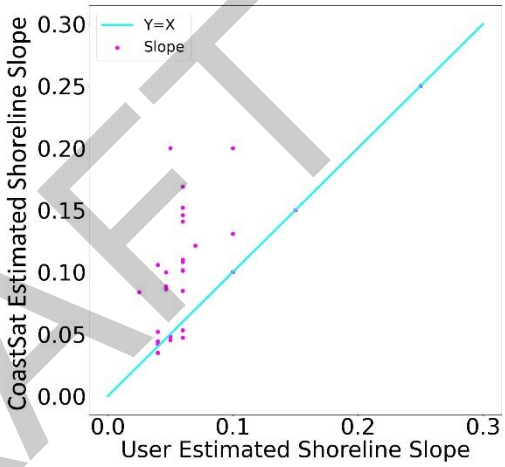

Figure 19. CoastSat-generated slopes versus user-selected slopes.

To investigate how slope influences shoreline accuracies, results using the CoastSat-derived slopes were compared to results using the field-measured slope (Fig. 20). Using CoastSat derived slopes caused slightly higher errors at 59% of our study sites, however, overall the horizontal differences in satellite versus ground truth shorelines was minimal (0.24 m) when compared across all sites (Fig. 20). Considering these results, at most sites, especially where conventional slope data is unavailable, the CoastSat slope function can be reliably used for shoreline extraction, despite its likely poor representation of true slope, which suggests at least at the sites tested here, slope does not exert a strong control on shoreline position accuracy. Notably, Vos et al. (2019) found no significant improvement of shoreline accuracy by using time-varying slopes instead of a time-averaged slope at Narabeen, AU. Furthermore, at the same site

using CoastSat.PlanetScope, Doherty et al. (2022) found using time-varying beach slope decreased shoreline position accuracy.

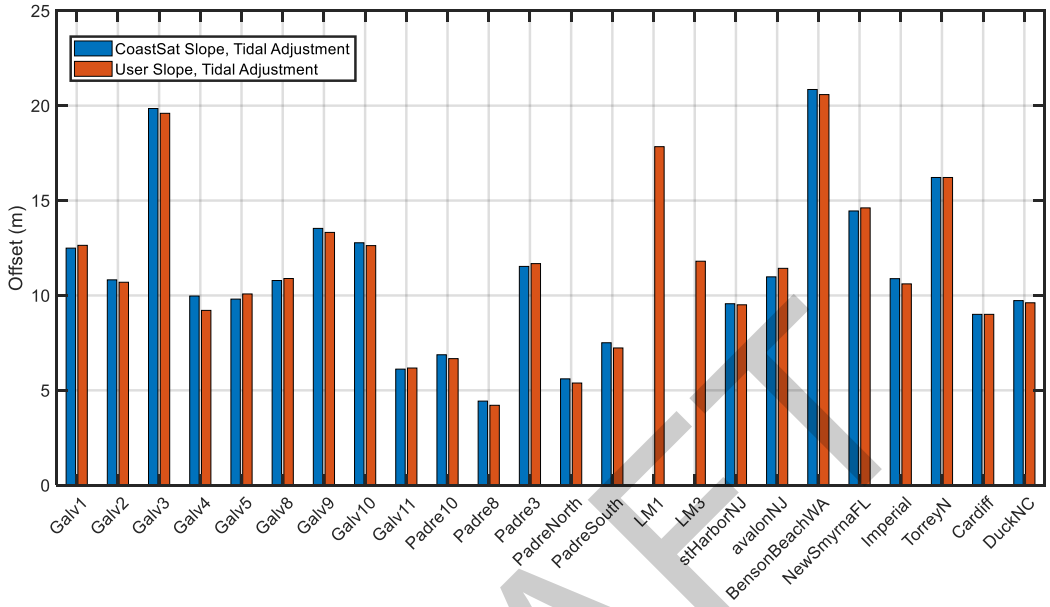

Figure 20. Summary of shoreline offsets for CoastSat-generated slopes (blue) and user-selected slopes (red).

4.4 Tidal Correction Influences

Shoreline position also fluctuates depending on the tidal stage. We assessed the influence of the tidal correction on shoreline positional accuracy in part because some users may be located in areas that do not have hydrodynamically proximal water level gages or predictions. Also, if the tidal correction only provides minimal shoreline accuracy improvement, users could opt to forego the tidal correction step.

For context, the study sites spanned a tidal range between 0.74 m and 3.10 m. And for clarification, the Great Lakes sites have no tides so the tidal corrections were not evaluated. Overall, the tidal correction lowered the mean shoreline position error at 82% of the sites (Figs. 21 and 22) with a reduction of -1.24 m in mean horizontal difference between satellite and ground truth shorelines. The largest accuracy improvements from tidal corrections occurred at three mesotidal sites: Avalon, NJ (- 4.22 m), Stone Harbor, NJ (- 2.75 m), Cardiff (-2.71 m); the microtidal Galveston (-3.36 m), and the macrotidal site of Benson Beach, WA (2.32 m).

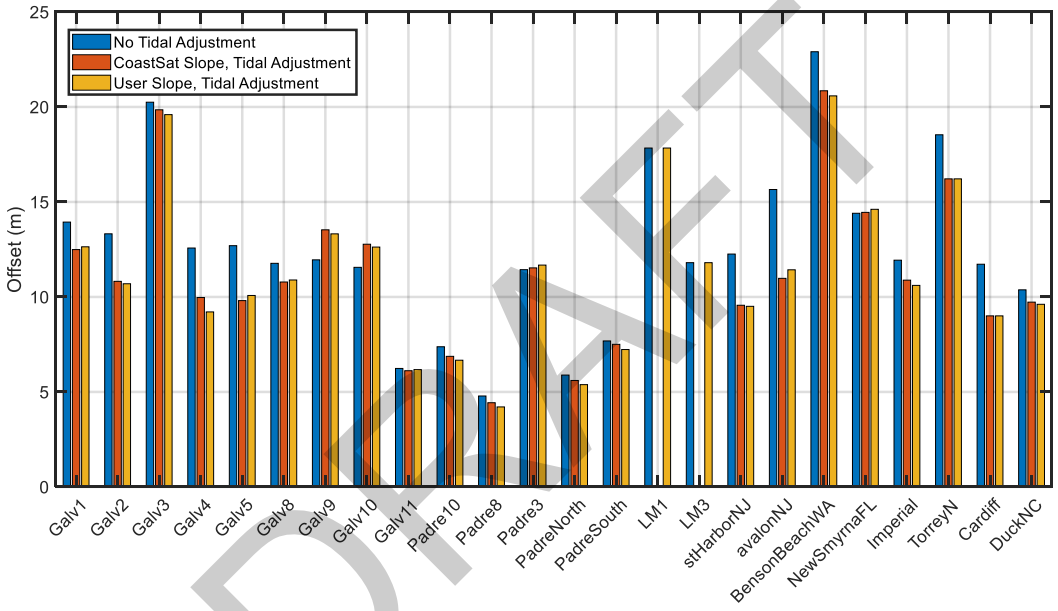

Figure 21. Bar plot showing satellite shoreline position accuracies without any tidal correction (blue), with a tidal correction using CoastSat slopes and tidal correction with user slopes.

Across sites for all reference times the mean horizontal difference was 12.45 m without the use of tidal correction (Fig. 21). When tides were corrected with the built-in CoastSat.Slope function to determine the beach slope along which to shift the shoreline, the mean horizontal difference was reduced 11.0 percent to 11.08 m. With the inclusion of a user given slope, determined by ground truth data and associated reports, the mean horizontal difference is reduced to 11.21 m. With the use of user estimated slopes and tidal correction sites varied from 4.2 to 20.6 meters of horizontal difference between the satellite derived shorelines and the reference data.

It is important to note that finding an open coast tidal station that is hydrodynamically proximal to your study site is crucial for proper tidal correction. We initially used an automated approach to select simply the closest tidal stations to each site; however, several of those selections were in inlets, bays or inshore which resulted in high shoreline position errors since the timing and magnitude of the tidal correction in those areas are not reflective of the open coast.

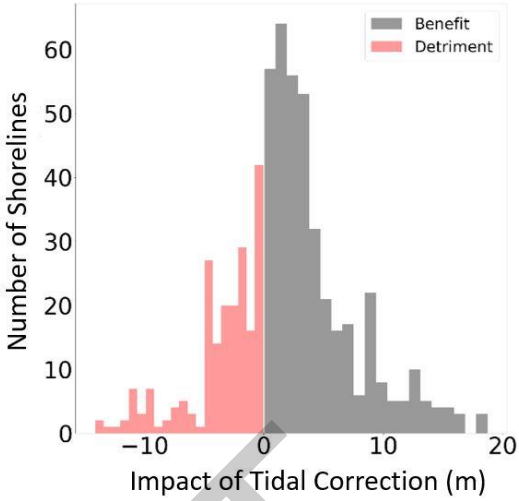

Figure 22. Impact of tidal corrections where grey positive values reflect the amount of improvement in meters after a tidal correction. Reds represent instances where tidal correction decreased accuracy,

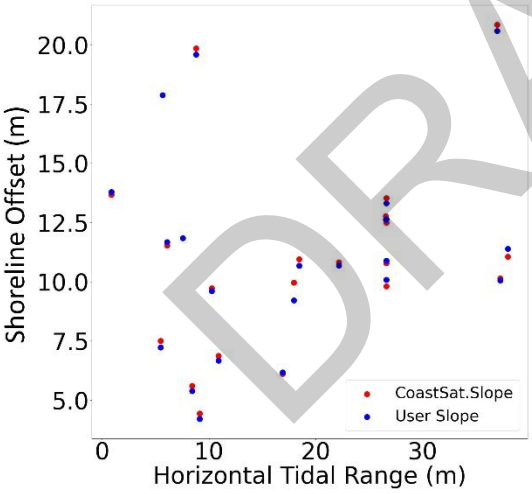

Figure 23. Shoreline offset versus horizontal tidal range generated from CoastSat slopes (red) and user slopes (blue).

We also examined shoreline accuracies relative to different tidal ranges. When the tidal range is combined with the site slope to calculate a horizontal distance, or horizontal tidal envelope, there appears to be a weak correlation with satellite shoreline accuracy, where generally larger horizontal tidal envelopes have higher shoreline position error (Fig. 23). Furthermore, Figure 23 highlights the general trend in slightly lower shoreline errors associated with user versus CoastSat slopes.

Lastly, we assessed shoreline positional error relative to tidal range and satellite mission. Figure 24 shows no apparent link with these parameters. Coincidentally, Landsat 5 encompassed the majority of our comparisons of satellite-derived shorelines and ground truth surveys at lower tide range sites (Fig. 24).

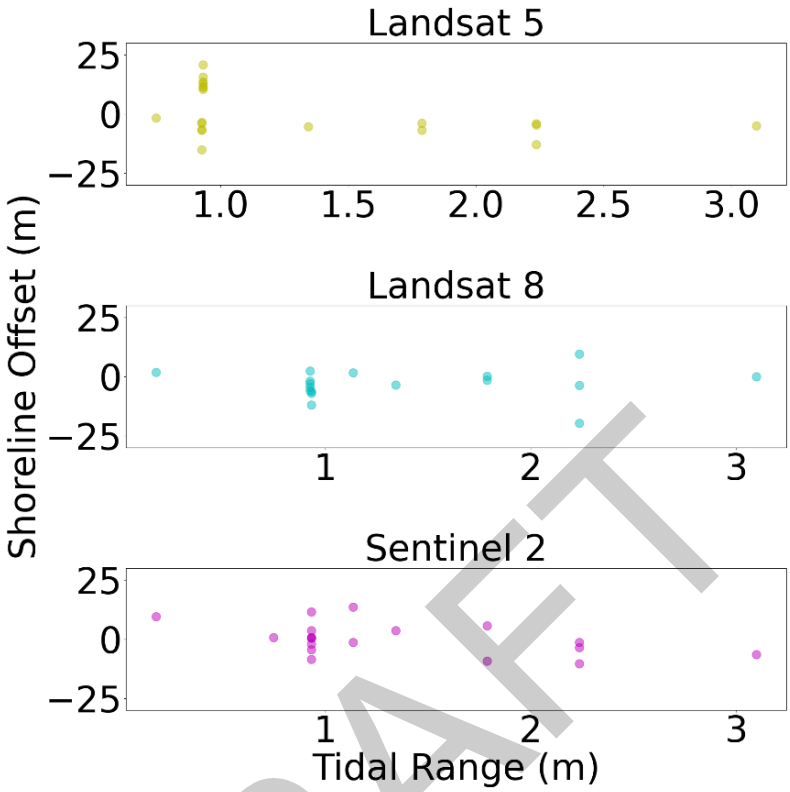

Figure 24. Shoreline offsets across all sites relative to tidal range and satellite missions.

4.5 Wave Runup Corrections

While CoastSat incorporates tidal corrections based on image capture time, it does not account for wave processes and high frequency swash motions (i.e. setup, runup, rundown, infragravity). An instantaneous satellite snapshot may occur during wave runup or rundown, yet this is not known, thereby leading to challenges in integrating a wave correction. Furthermore, wave and swash processes generally vary alongshore, adding even more complexity (e.g., Stockdon et al., 2007). To address these concerns, we focused on five sites with robust available wave data and frequent reference data – Duck, Benson Beach, Cardiff, Imperial and Torrey Pines North.

Likely due to the high frequency of swash motions, results showed adding adjustments for runup improved shoreline accuracy at 60% of the sites (Figs. 25 and 26). We suspect that this is in part due to the randomness of waves relative to image capture time. Furthermore, adding wave runup offsets effectively can only shift a shoreline more seaward, so if it was already too far seaward, runup would exacerbate the shoreline position accuracy. Figure 26 shows that when combining the site slope with runup to create a runup envelope, roughly half of the ground truth comparisons improve in terms of accuracy and the other half have higher shoreline offsets. Future work could explore creating a shoreline position envelope based on the tide elevation + setup +/- $S/2$, where S is the significant swash height from Stockdon et al., 2006, for example. Satellite shorelines could then be assigned a potential water-level related uncertainty and considered accurate if surveyed shorelines fell within this envelope.

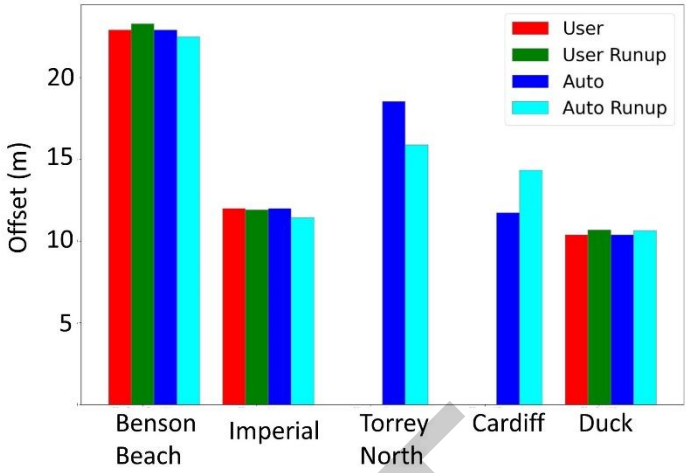

Figure 25. Results of runup corrections at five test sites. Red indicates user slope with no runup correction, green is user slope with runup correction, blue is CoastSat slope with no runup correction and light blue is CoastSat slope with runup correction.

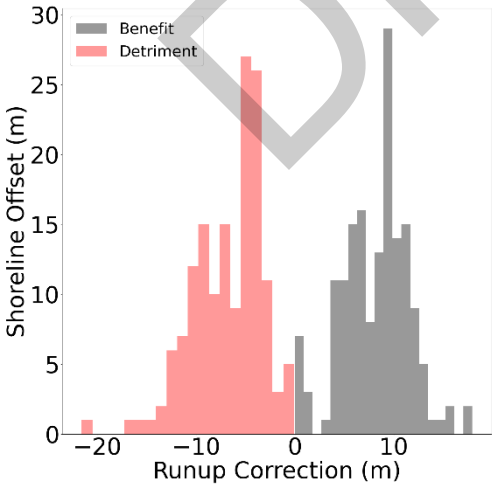

Figure 26. Shoreline offsets (m) for all runup test sites versus horizontal wave runup envelopes (m).

We also evaluated runup corrections during different seasons (Fig. 27) and wave conditions (Fig. 28). Figure 27 shows some weak correlation between seasons and shoreline accuracy where the better accuracies are

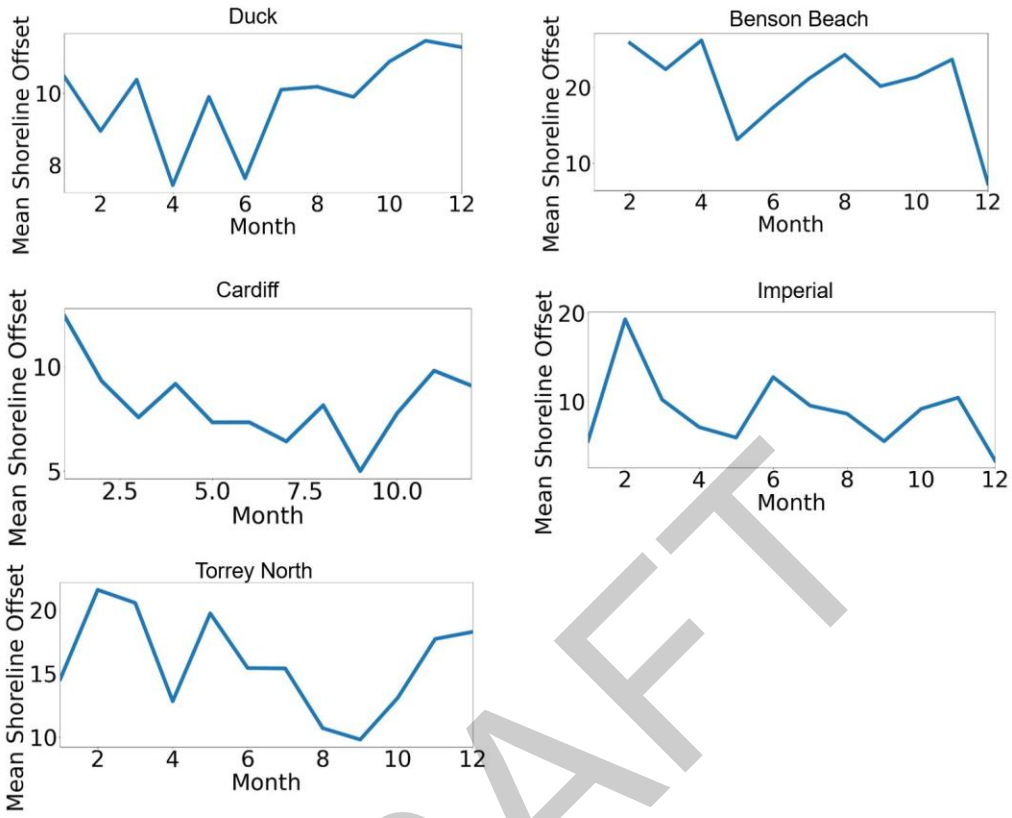

Figure 27. Average monthly wave height (m) versus mean shoreline offset (m) across five runup correction test sites.

found during summer months and the lower accuracies are during the stormier winter season. Based partly off seasonal trends and results of Figure 28, we considered implementing runup corrections only during stormy intervals, yet determining a specific wave height threshold is also challenging and would likely need to vary site by site. At Duck, for example, implementing runup correction only when waves were > 1.5 m, caused overall improvement of 0.5 m (9.6 m to 9.1 m) in mean horizontal difference between ground truth and satellite shorelines. Yet, Figure 28 shows there is no clear link of shoreline accuracy improvements from wave corrections in high and low wave conditions at other sites. Past work aimed at reducing noise in swash motions has used composite images averaged over long time intervals or elevation correction models

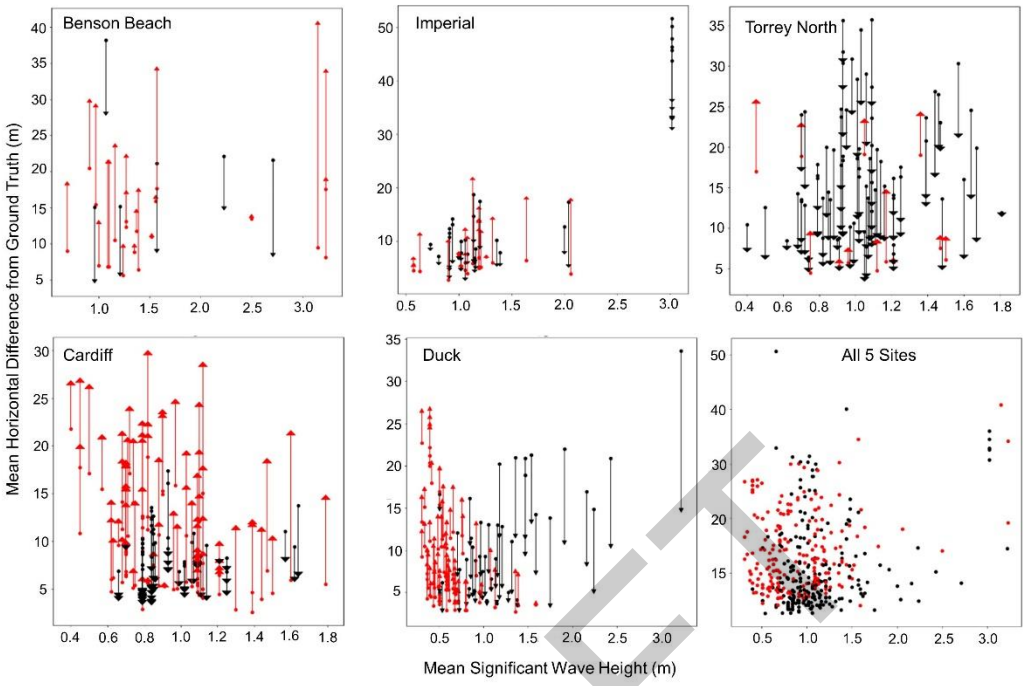

Figure 28. Summary for runup corrections at all five sites where the y-axis is mean shoreline satellite position error and x-axis is wave height. The dot/arrow combinations show the magnitude of error increase (red) and decrease (black) where the dot represents the initial shoreline error prior to runup correction.

(Almeida et al., 2021; Bishop-Taylor et al., 2021; Luijendijk et al., 2018). Castelle et al. (2021) used CoastSat at Truc Vert, France and applied an elevation correction model which was successful in reducing satellite-derived shoreline position error by half. However, this is in part attributed to the slope (0.05), interannual variability in waves (Hs of 1.1 m in summer and Hs of 2.4m in winter), and meso-macrotidal regime (tidal range up to 5 m) which make runup effects more pronounced at this site. On the contrary, using CoastSat with PlanetScope imagery (3 m resolution) at Narabeen-Collaroy, Australia and Duck, NC, Doherty et al. (2022) found implementing time varying runup only caused negligible improvements on satellite-derived shoreline accuracy (<1%). Doherty et al. (2022) suspect the results are due to the steeper nature of the coastline (average intertidal slope of 0.09), less interannual wave variability and microtidal regime (mean spring tidal range of 1.3 m), that make the shoreline less susceptible to large horizontal movements of swash motions. More research is still needed to determine if these cases of runup correction are site specific. Not having to account for wave processes

would be advantageous since nearshore, high resolution wave data may not be available or difficult to obtain in many locations.

5 Shoreline Trend Comparisons

In this chapter we examine the twenty-year trends derived from satellite imagery and compare them to ground truth data. We first explore how accuracy varies with time, then discuss the trends in more detail at selected sites. Specifically, we address how satellite trend data can be used to monitor subaerial equilibration and evolution of different coastal management strategies and for storm impact/recovery assessments.

5.1 Temporally Variable Confidence

After examining the accuracy of the individual shorelines, the ability to estimate shoreline evolution trends from the collection of shorelines was assessed. To do this, the slope of the shoreline position relative to the transect root as a function of time was assessed for every combination of reference survey times, inclusive of surveys occurring between those pairs. A corresponding set of shorelines was selected from the satellite derived collection spanning the same time period. Figure 29 illustrates this concept where both short and long trends were compared to reference data.

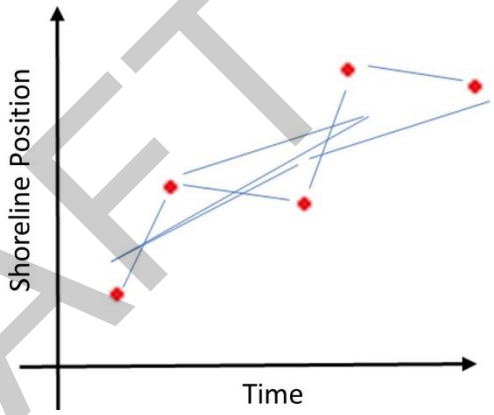

Figure 29. Schematic representing the way in which different time interval trends (blue) were examined relative to reference data (red crosses).

As the number of passes included in the subset of the collection increased, the accuracy of the trend improved rapidly (Fig. 30). With a subset encompassing 200 days of data, the mean difference in the trend was -3.10 m/yr, with a standard deviation of 44.07 m/yr (Fig. 30). With a subset encompassing 650 days of data, the mean difference in the trend was -0.04 m/yr, with a standard deviation of less than 9.74 m/yr (Fig. 30). These trend accuracies related to time may be important to consider for certain users when selecting time intervals. Examples of the shoreline trends and management applications of these data are explored at select sites in the following section. We will show satellite-derived shorelines are able to quantify annual cycles, response to nourishment and storm events, and long term trends, all of which can improve management of coastal resources.

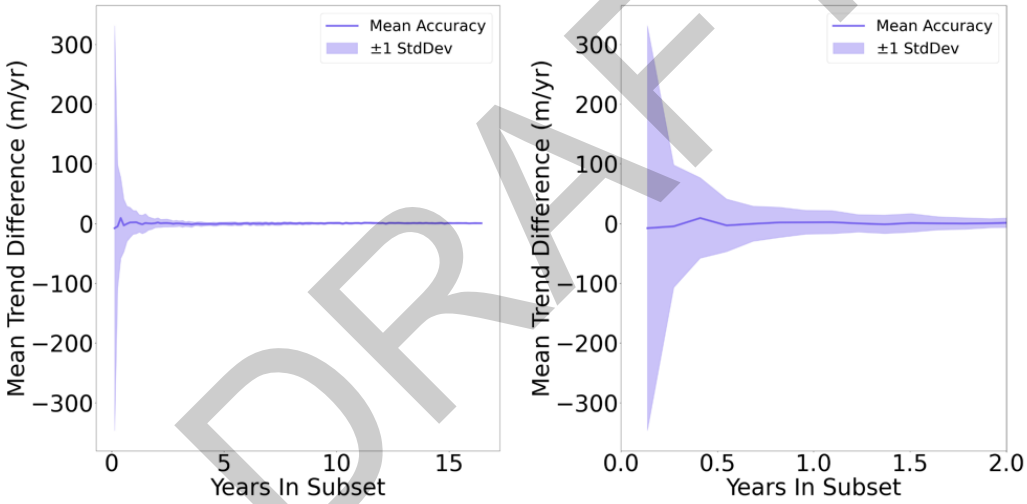

Figure 30. Trend differences (m/yr) of satellite-derived shorelines compared to ground truth shorelines relative to time in (years). The second panel is a zoom of two years.

5.2 Harvey Cedars

The Harvey Cedars test site is characterized by a narrow beach from 2000 to 2008 with interannual variability likely driven by seasonality (Fig. 31). During this interval, the satellite-derived data show poor alignment with ground truth data with an offset of ~25 m, likely due to the GEE mission offset issue. However, post-2010, the data show good agreement,

especially during beach nourishment projects. From the satellite data, we can easily quantify changes to the beach in response to management actions. The first major beach nourishment (2,991,805 CY) during the 20-year study period was conducted in 2010, showing a pronounced increase in beach width on the order of 110 m. After the project was constructed, equilibration was accelerated by Hurricanes Irene (2011) and Sandy (2012). Over a period of 2.8 years, the beach width was reduced by

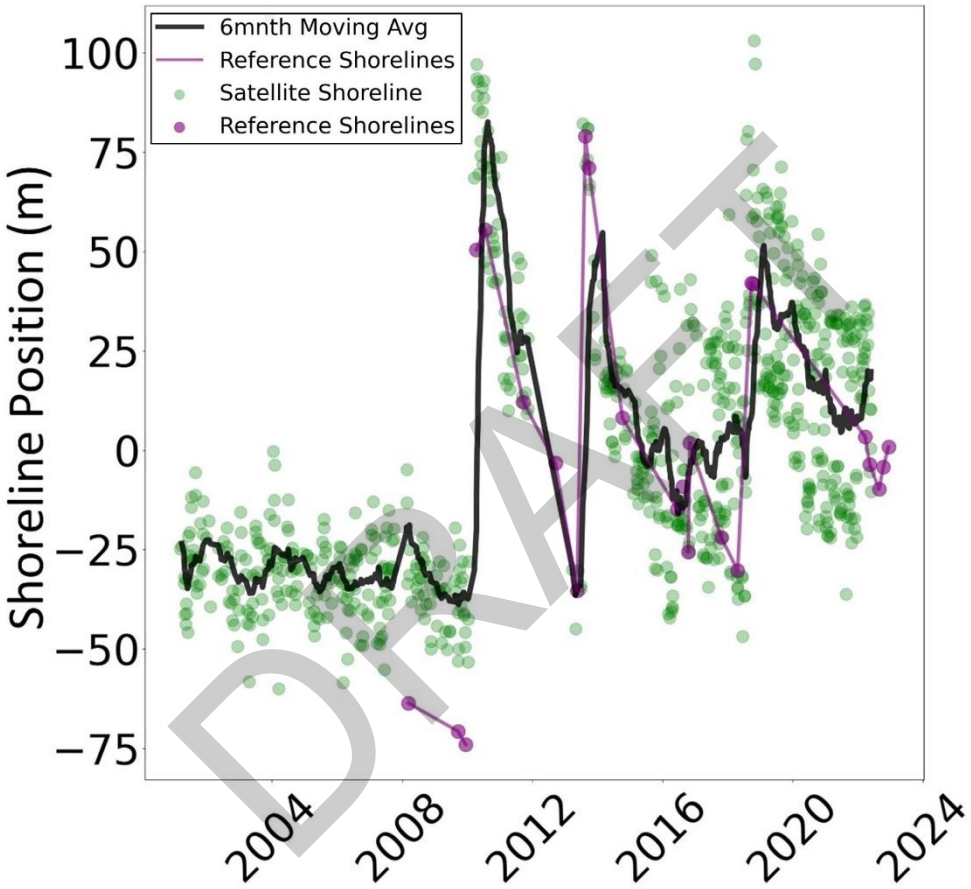

Figure 31. Twenty-year shoreline trends at Harvey Cedars Pilot site.

116.1 m to pre-project width, at a high rate of -41.76 m/yr. Following Hurricane Sandy, an emergency repair nourishment was conducted which returned the beach to roughly the 2010 post-nourishment width. Shoreline retreat at a rate of 19.35 m/yr followed but the beach remained ~20 m wider than the period from 2000-2008. The last nourishment occurred in 2018 and by 2.4 years later had equilibrated to pre-repair beach width (-18.78 m/yr). The satellite-derived shoreline record thus can be used to demonstrate and quantify the impacts of coastal management on the

shoreline position. Specifically, that active nourishment and coastal management has resulted in a beach that is on average 20-m wider in the last 10 years when compared with the un-nourished beach, even during a period which saw an extreme storm. These data can help communicate the value of active coastal management and enable decision makers to evaluate if the costs are worth the benefits. In addition, the long satellite record can be used during feasibility studies to quantify the background natural variability to the system prior to funded monitoring efforts.

The last, most recent management project at Harvey Cedars was the emplacement of a nearshore berm as beneficial use of dredged material from a federal navigation project in response to an erosional hotspot identified by the Federal Coastal Storm Risk Management (CSRM) project. In the summer of 2021, 83,300 m^3 was dredged from Barnegat Inlet and placed in the nearshore (2.75 m depth) of Harvey Cedars. Work to analyze the evolution of the placement is ongoing using in situ hydrodynamic sensors and satellite-derived shorelines (McGill et al., 2022; accepted). Preliminary results show a lagged widening of the shoreline at the adjacent beach of 5-10 m (Fig. 32). These satellite data can potentially reduce the costs associated with monitoring coastal management actions and are capable of capturing the shoreline response from a small scale engineering project.

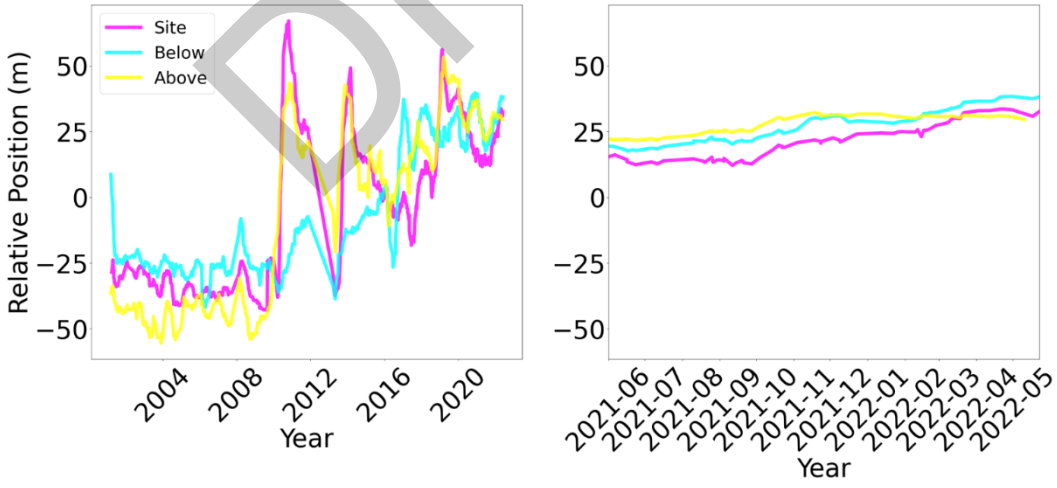

Figure 32. Harvey Cedars satellite shoreline trends within the nearshore berm placement zone (purple), below (south) the placement site (blue) and above (north) the placement site (yellow).

5.3 South Padre Island, TX

The South Padre Island test site is an example of the paucity of available ground truth survey data to districts. When compared to the five reference shorelines, the satellite derived shoreline positions and trends align well, showing a long-term accretion trend at the site (Fig. 33). The satellite data allows for a much more complete depiction of the shoreline evolution at the site. For example, the gap in survey data between 2012 and 2016 fails to capture the interannual/seasonal beach width fluctuations that are on the order of 10 m (Fig. 33). In addition, between the last two ground truth shoreline data points, the maximum beach width excursion over the two-decade period is missed.

From a coastal engineering and management perspective, the utility of Satellite-derived shoreline monitoring is evident. Most nourishments at South Padre Island were small to medium scale (<500,000 CY) navigational channel dredging and sediment re-use episodes. The beach width generally increased by 10-20 m following these projects (e.g., Fig. 33; peaks in 2005 and 2011). The most recent federal shore protection project nourishment event is also apparent in 2021 with the increase in beach width on the order of 10 – 20 m. The strongest storm impacts over this time interval were caused by Hurricane Dolly in 2008, which left a marked erosional signal of ~30 m followed by rapid shoreline recovery. Hurricane Hanna in 2020 triggered the notable reduction in beach width (~25 m) as shown by the satellite data. Satellite shorelines can thus be used to inform adaptive management studies by evaluating if assumptions of equilibration rates and recovery intervals from storms within USACE planning tools (e.g. Beach-FX) have been tuned appropriately for a given site.

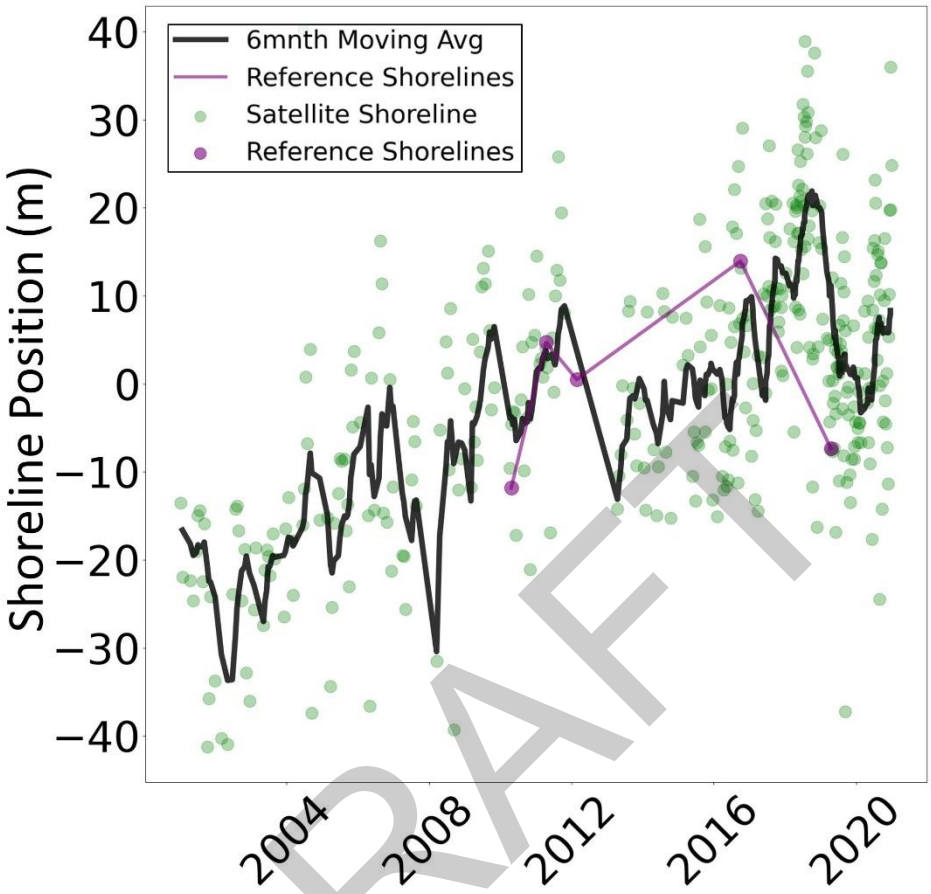

Figure 33. Twenty-year shoreline trends at South Padre Island, TX (North).

5.4 Duck, NC

The Duck 20-year trend data shows frequent large changes in beach width, primarily driven by extratropical and tropical storm events. Figure 34 highlights the abundance survey ground truth data, that generally aligns well with the satellite-derived shorelines. Some discrepancies are evident during periods when the survey data show the widest shorelines (e.g., Fig. 34; 2003 and 2011). There is also significant noise in the satellite data and examining the six-month moving average line is especially useful for tracking bulk shoreline oscillations (Fig. 34; black line).

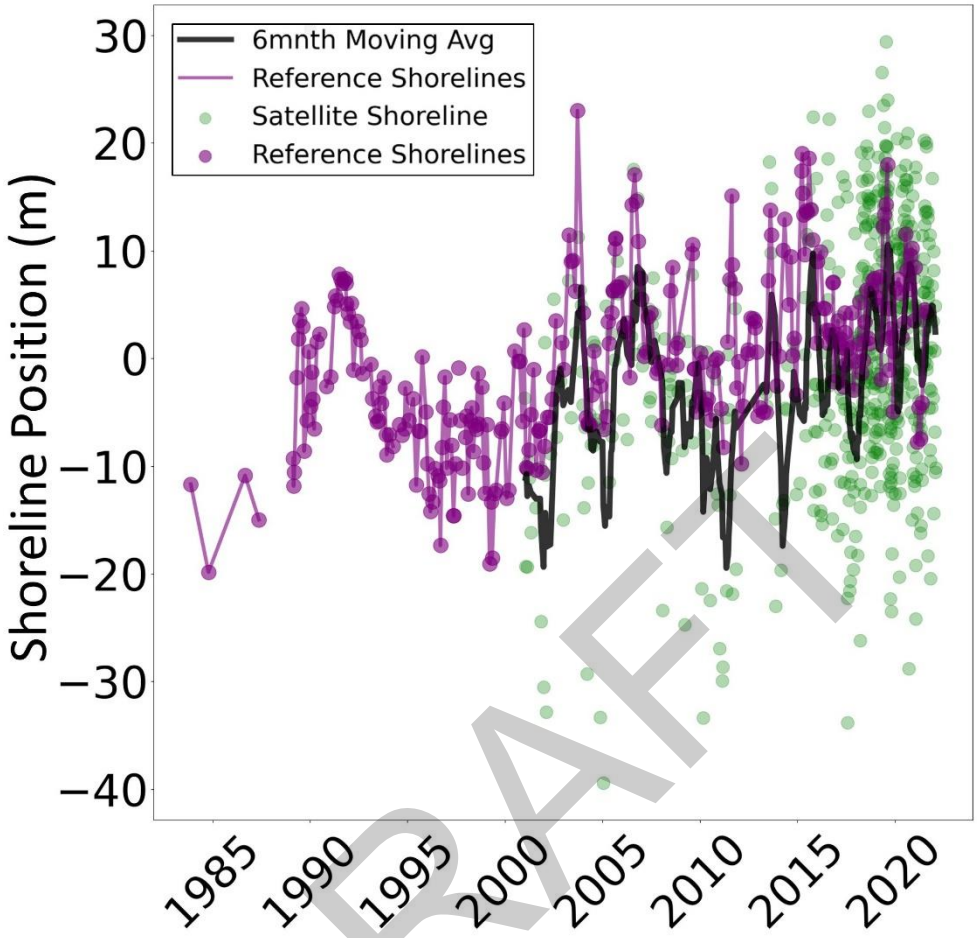

Figure 34. Twenty-year shoreline trends at Duck, NC.

Several storm impact and recovery cycles are clearly shown in satellite-derived shoreline data. For example, Hurricane Dorian in 2019 caused shoreline retreat on the order of 20 m, but one year following the shoreline recovered to pre-storm width. The most recent time period is predominantly characterized by severe nor'easter impacts where shorelines receded 10-15 m from storm impacts. These extratropical impacts span long duration stormy periods and often cause more erosion than tropical systems, also noted by Cohn et al., (2022).

The Town of Duck conducted the first beach nourishment project in 2017. To analyze the specific impact of the nourishment, timestacks were created in which the differences in the cross-shore position of the shoreline were normalized by the behavior of the shoreline outside the region of influence of the management action. The timestack (Fig. 35) shows the increase in shoreline width following initial construction that started within the monitored area in May 2017. Immediately after construction, alongshore dispersion of the nourishment to the south occurs beyond the nourishment project bounds (also shown in Cohn et al., 2022). Figure 35 shows erosion within the nourished zone beginning ~11 months after project construction (Fig. 35). Erosion was most severe from late fall nor'easters (Cohn et al., 2022). The large regional extent of the satellite-derived shorelines enabled analysis of the influence of the nourishment to the adjacent coastal areas. The ability to capture temporally dense nourishment evolution, the timing of subaerial equilibration and longshore dispersion rates and diffusion beyond project bounds may be particularly useful to coastal managers and planners designing nourishment projects and developing adaptive management plans.

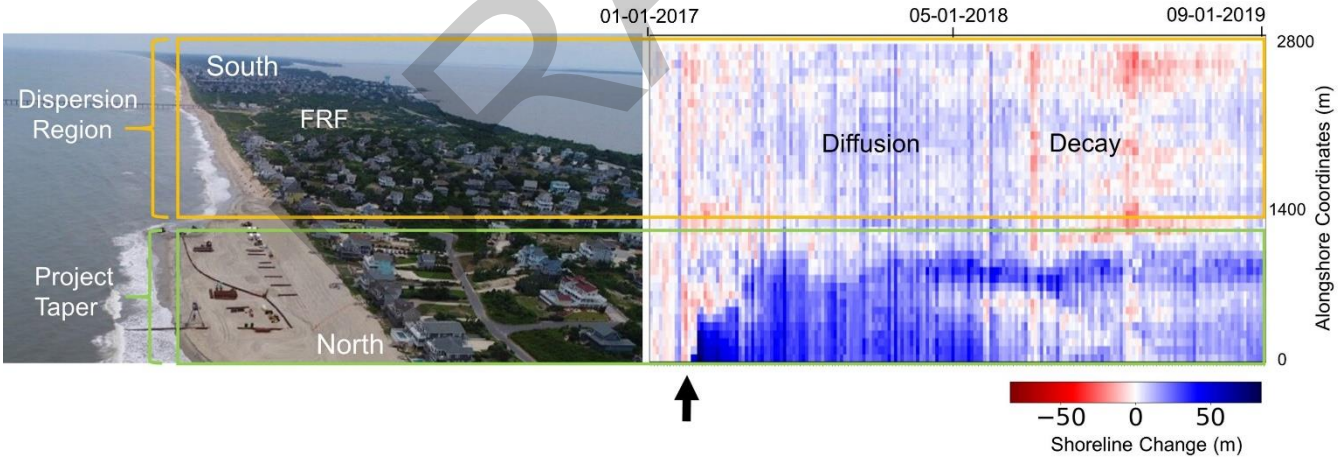

Figure 35. Satellite shoreline timestack from Duck, NC where the right y-axis represents the alongshore coordinates (m) and colors represent shoreline recession (red) and advance (blue). The differences in cross-shore position of shorelines through time are normalized by the behavior of a shoreline outside the region of influence of the management action. The black arrow indicates the start of the 2017 beach nourishment project.

5.5 Avalon, NJ

When compared to the ground truth survey data, the satellite-derived shoreline trends show good agreement in Avalon, NJ (Fig. 36). The periods of time with the widest and narrowest beach widths align well and the satellite imagery is capable of detecting the frequently changing beach widths. If only looking at survey data (purple dots) several major shoreline oscillations are missed; for example, there was a large gap in ground truth data from ~2004 to ~2009 which did not capture the shoreline recovery period prior to 2009 (Fig. 36). Another example occurs around 2010, where despite more frequent survey data (Fig. 36, fourth and fifth purple points), a strong erosional perturbation is missed over a short time interval, including observations of when the shoreline was in its most erosive state over the course of two decades.

The decadal time series from Avalon, NJ captures several interesting nourishment and storm impact/recovery cycles and highlights the value of high

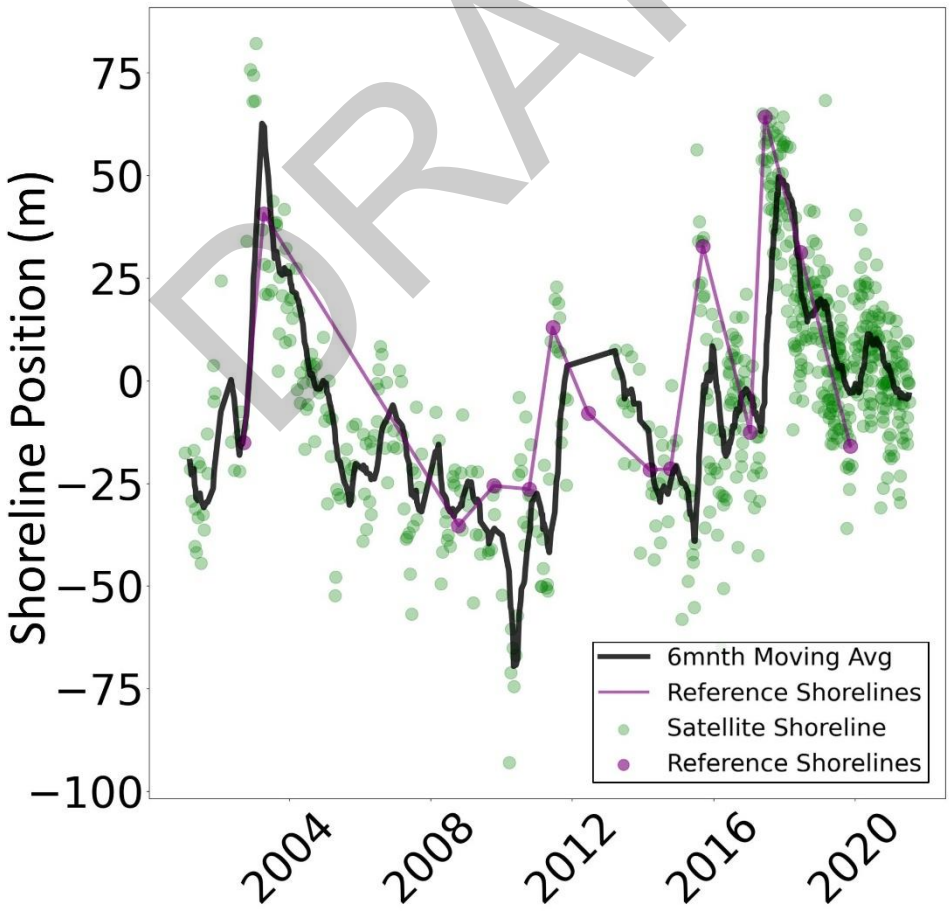

Figure 36. Twenty-year shoreline trends at Avalon, NJ.

temporal frequency monitoring capability for coastal management and engineering project applications. The large 4,090,000 CY beach nourishment in 2003 is evident in the satellite shoreline positions. By 9/15/2005, the satellite-derived shorelines show a narrowing of the shoreline and return to pre-project beach width. Following this large nourishment, equilibration occurred resulting in shoreline recession at a rate of ~37.6 m/yr. This high rate of shoreline retreat following nourishment is likely attributable to a very active 2004 hurricane season which included impacts from four storms: Bonnie (August), Charlie (August), Gaston (August) and Ivan (September). Prior to the next major nourishment in 2011, the erosion from Hurricane Barry in May 2007 is clear (8 m shoreline retreat). After significant beach narrowing around 2010, two large nourishments followed in 2011 and 2013 totaling 2,040,583 CY.

A gap in satellite imagery does not allow for an assessment of the 2011 nourishment episode, but when examining the two nourishments combined, the beach returned to pre-nourishment width after 3.6 years, which is roughly equivalent to a shoreline recession rate of 11.9 m/yr. While episodic erosion is missed from Hurricane Sandy (2012) due to lack of imagery, we suspect Hurricane Irene and Sandy were responsible for significant sediment loss during this nourishment cycle (Fig. 36). Figure 37 displays the ability of satellite-derived shoreline analysis to capture hurricane impacts, showing an erosional signal of ~50 m during Hurricane Irene. This suggests the potential to use satellite imagery in post-storm assessments to quantify impacts to federal project sites and inform applications for emergency relief efforts. The last notable nourishment of 1,636,685 CY was conducted in 2017. Over the next 2.25 years, the beach equilibrated to pre-project width, at a recession rate of 23.2 m/yr.

Figure 37. Satellite shorelines spanning from 8/24/2011 to 9/16/2011 with early dates in blue and post-Irene (8/25/2011 impact) shorelines in red. Note shoreline erosion on the order of ~50 m.

5.6 Torrey Pines, CA

Shorelines at Torrey Pines, CA exhibit high annual and interannual variability (generally 10-20 m) which the satellite-derived shorelines are capable of capturing (Fig. 38). In addition, this site contains cobbles at times which provides an interesting test of the algorithm on an atypical mixed-sediment shoreline. The largest trend discrepancies occur around 2012 when ample usable imagery was lacking.

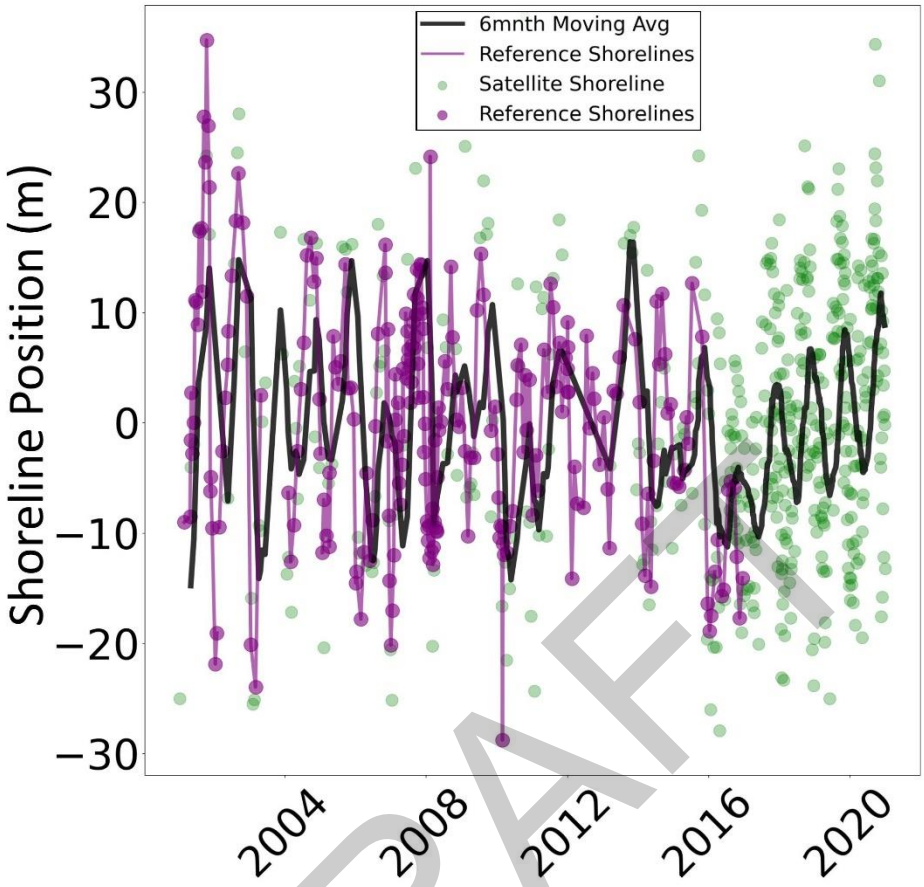

Figure 38. Twenty year shoreline trends from Torrey Pines North.

5.7 New Smyrna Beach, FL

New Smyrna Beach, FL presented the opportunity to leverage other coastal imaging work monitoring a nearshore berm placement and to compare satellite-derived shorelines to other visually-based digitized shorelines from a mini-Argus station (Bruder et al., 2019). This site thus represents a unique example when compared to all other locations, which used 3D topographic data with vertical datum-based shorelines. As noted in the site description, the manual digitization approach to estimating shoreline position has a precision on the order of 10 m and needs to be accounted for accordingly when comparing to satellite-derived shoreline estimates (Onnink, 2020). It should be noted that the nature of the shoreline at this site presents challenges in visual delineation because there is a wide saturated zone with dark coloration. Therefore we would expect uncertainty with any visual shoreline approach.

Argus imagery was used to produce timestacks to help assess how the nearshore berm impacted the nearshore system and shoreline. As mentioned for Duck, these timesatacks are normalized relative to shorelines outside of the area influenced by the management action. The mini-argus timestack is strikingly similar compared to the satellite-derived timestack, emphasizing the utility for monitoring various engineering projects like nearshore berms (Fig. 39). Both the mini-Argus and satellite derived shorelines show the increase in offshore movement of the shoreline in the lee of the nearshore berm. Also note the additional context provided by the satellite data that extends well before and after the mini-argus deployment. While this is not intended to suggest satellites could replace higher resolution systems like mini-argus that have additional valuable functionality (e.g., timex for wave breaking), it does show the power of publicly available satellite imagery.

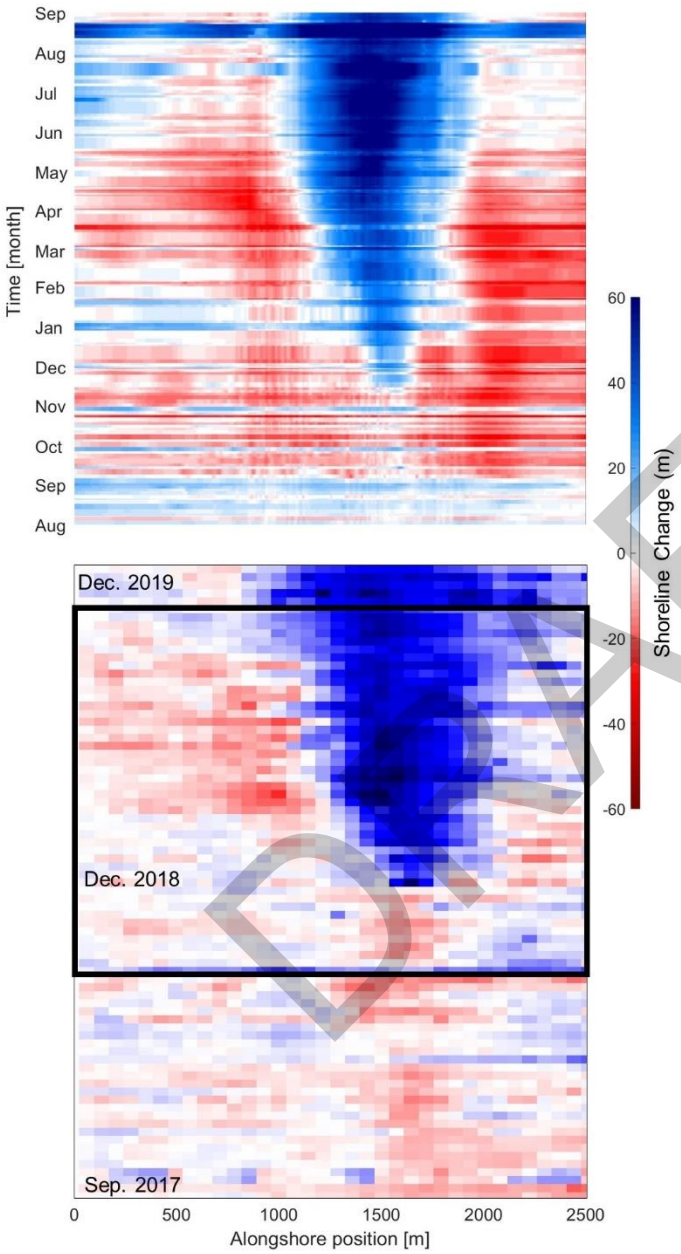

Figure 39. Mini-argus generated shoreline timestack for nearshore berm monitoring (top) and satellite-derived shoreline timestack (bottom). The black box represents the time interval of the mini-argus deployment as reflected in the top panel. Sediment was placed from 1200 m to 1800 m in the alongshore.

5.8 Wrightsville Beach, NC

While it is not included in earlier analysis, this site was investigated in Brown (2021) and is a good example of frequent large scale federal beach renourishments. Wrightsville Beach received its first nourishment in 1939, completed the first Coastal Storm Risk Management project in 1965, and was reauthorized in 1986 to continue on a four-year renourishment cycle. These cycles allow for the opportunity to quantitatively evaluate exponential subaerial nourishment decay rates, which may assist with project planning and volume optimization (Fig. 40).

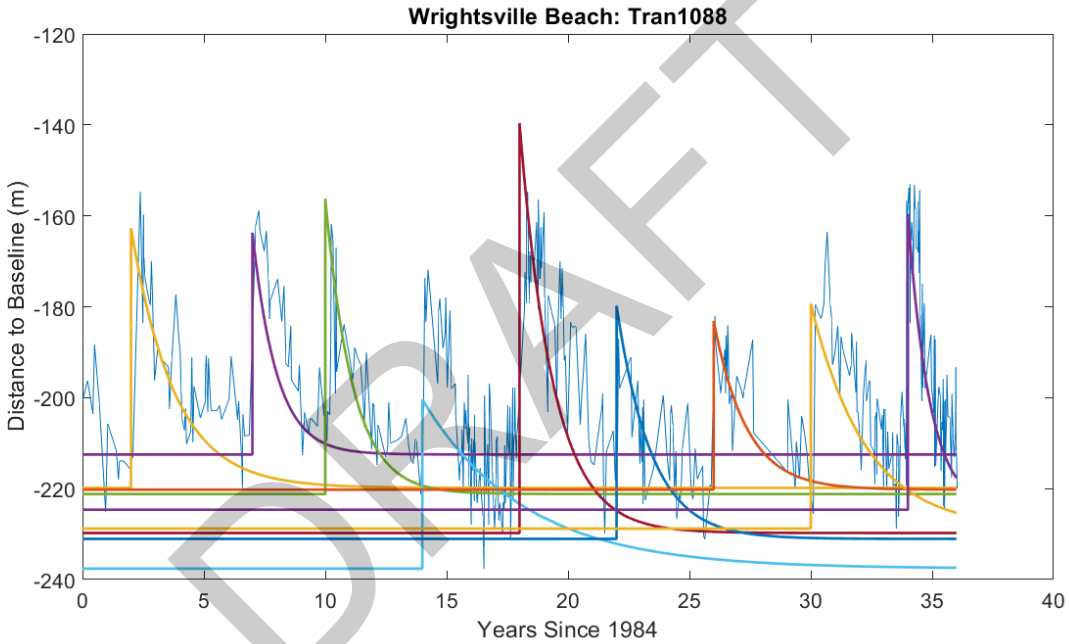

Figure 40. Wrightsville beach shoreline evolution from renourishment cycles since 1984. The colored lines represent exponential decay of the subaerial beach after each project.

6 Conclusions and Recommendations

6.1 Conclusions

The ERDC research team conducted accuracy testing of the CoastSat algorithm at a total of 37 sites selected across the nation in coordination with District partners. Specific conclusions are as follows:

- Mean alongshore horizontal offsets of satellite-derived shorelines compared to ground truth surveys ranged from 4.2 m to 20.5 m, with an overall mean of 11.32 m and slight onshore bias of -3.51 m. Sentinel-2 was most accurate with a mean alongshore horizontal offset equal to 8.86 m, followed by Landsat-5 (10.52 m) and Landsat-8 (10.57 m).

- Tidal corrections improved accuracies at 82% of our sites. Selection of nearby open coast tidal stations is challenging in some locations, yet it is critical for improving satellite-derived shoreline accuracies.

- While there were some discrepancies in CoastSat-generated slopes compared to user defined slopes, the impact on shoreline accuracy was negligible whereby user-defined slopes improved overall accuracy by 0.24 m. This is advantageous as it shows CoastSat slope function can be used when no field or ground truth derived slope information is available.

- Implementing wave runup corrections slightly improved accuracy at 3 out of 5 test sites where robust wave data was available. Investigation is ongoing to test other runup/setup correction approaches and determine site specific dependencies.

- 20-year satellite-derived shoreline trends generally agree well with ground truth shoreline trends. With 200 days of data, the mean difference in the trend was -3.10 m/yr, and with a subset encompassing 650 days of data, the mean difference in the trend was -0.04 m/yr.

- ERDC added several improvements outside of the typical CoastSat workflow including more efficient image sorting, tidally shifted

shoreline shapefiles, runup corrections and various analysis products.

- Satellite-derived shorelines were able to quantify a variety of impacts from management actions including subaerial beach nourishment equilibration, diffusion and decay, shoreline response to small nearshore berm placements, and background/natural versus engineered shoreline variability. In addition, CoastSat captured many storm impact and recovery cycles.

- This satellite-derived shoreline approach represents a free and powerful data source for Districts and coastal practitioners that can provide both decadal and short-term shoreline insights at broad spatial scales. These satellite data can potentially reduce the costs associated with monitoring coastal management actions, improve project design and inform adaptive management and feasibility studies. The development of a user-friendly desktop tool to make this technology more accessible is ongoing.

6.2 Recommendations

The research team suggest a primary takeaway from this effort is that CoastSat shoreline accuracy is strongly linked to satellite pixel resolution. Despite the capability to operate at a sub-pixel scale, we hypothesize that consistent accuracy < 5 m would be difficult to achieve without improved satellite resolution. Only one test site (South Padre 8) was <5 m accuracy.

Other work by Doherty et al. (2022) focused on PlanetScope imagery with a resolution of 3.0 m at Duck and other sites and found RMSEs ranging from 3.5 m to 5.1 m. Doherty et al. (2022) state: “The increase in accuracy obtained by PlanetScope imagery is subsequently sufficient to capture smaller-scale variability at the sub-annual or seasonal timescales, particularly considering the generally smaller magnitude of shoreline variability at Duck relative to Narrabeen. This was identified as a key limitation of applying *CoastSat* and Landsat/Sentinel-2 at less dynamic sites (Vos et al., 2019a).”

There are other higher resolution imagery candidates to consider as well including Maxar Worldview-3 (pixel resolution = 0.31 m; Turner et al., 2021) and Dove Cubesats that are capable of multiple passes per day which could potentially help to reduce shoreline noise. These are currently not compatible within the CoastSat workflow.

References

Almeida, L.P., I. Efraim de Oliveira, R. Lyra, R. Scaranto Dazzi, V. Martins, A. Henrique da Fontoura Klein. 2021. "Coastal analyst system from space imagery engine (CASSIE): shoreline management module." *Environ. Model. Software* 140, 105033. https://doi.org/10.1016/j.envsoft.2021.105033.

Aronow, S., W. Fisher, J. McGowen, and V. Barnes. 1982. "Geologic Atlas of Texas, Houston Sheet: The University of Texas at Austin, Bureau of Economic Geology, scale 1:250,000, 1 sheet."

Bergsma, E., M. Sadio, I. Sakho, R. Almar, T. Garlan, M. Gosselin, and H. Gauduin. 2020. "Sand-spit evolution and inlet dynamics derived from space-borne optical imagery: Is the Senegal-river inlet closing?" *In:* Malvárez, G. and Navas, F. (eds.), *Global Coastal Issues of 2020. Journal of Coastal Research*, Special Issue No. 95, pp. 372-376. Coconut Creek (Florida), ISSN 0749-0208.

Birkemeier W, R. Dolan, and N. Fisher. 1984. "The evolution of a barrier island: 1930–1980." *Shore and Beach* 52: 2–12.

Bishop-Taylor, R., R. Nanson, S. Sagar, L. Lymburner. 2021. "Mapping Australia's dynamic coastline at mean sea level using three decades of Landsat imagery." *Rem. Sens. Environ* 267, 112734 https://doi.org/10.1016/j.rse.2021.112734.

Brown, S., University of North Carolina Wilmington M.S. Thesis, 2021. "Using satellite data and the Kalman Filter to improve analysis of historical shoreline trends from 1984 to the present and future projections along the U.S. Atlantic coast."

Brown, L., J. Brewton, J. McGowen, C. Proctor, S. Aronow, and V. Barnes. 1975. "Geologic Atlas of Texas, Beeville-Bay City Sheet: The University of Texas at Austin, Bureau of Economic Geology, scale 1:250,000, 1 sheet."

Bruder, B., K. Brodie, N. Spore, A. Renaud, and K. Hodgens, K. 2019. "Continuous monitoring of a nearshore berm placement at New Smyrna Beach, FL via coastal imagery." In Wang, Ping (University

of South Florida,U., Rosati, Julie D. (US Army Corps of Engineers, U., and Vallee, Matthieu (University of South Florida, U., editors, *Coastal Sediments 2019*, pages 2443–2457, Tampa/St. Petersburg, Florida. World Scientific.

Castelle, B., G. Masselink, T. Scott, C. Stokes, A. Konstantinou, V. Marieu, and S. Bujan. 2021. "Satellite-derived shoreline detection at a high-energy meso-macrotidal beach." *Geomorphology* 383, 107707. https://doi.org/10.1016/j.geomorph.2021.107707.

Chrzastowski, M., C. Foyle, and C.Trask. 1996. "Erosion and accretion trends along the Lake Michigan Shore at North Point Marina and Illinois Beach State Park. Year-1 (1995) Report of a Four-Year Study of Coastal Geology and Coastal Geologic Processes." *Illinois State Geological Survey*: 146.

Cialone, M., E. Thompson. "Wave Climate and Littoral Sediment Transport Potential, Long Beach Island, New Jersey." ERDC/CHLTR-00-21; U.S. Army Corps of Engineers Engineer Research and Development Center: Vicksburg, MS, USA, 2000; 75p. Available online: http://hdl.handle.net/11681/7451.

Cohn, N., K. Brodie, I. Conery, and N. Spore. 2022. "Alongshore variable accretional and erosional coastal foredune dynamics at event to interannual timescales." *American Geophysical Union Earth and Space Science*.

Dally, W., and D. Osiecki. 2018. Evaluating the Impact of Beach Nourishment on Surfing: Surf City, Long Beach Island, New Jersey, U.S.A. *J. Coast. Res.* 34, 793–805.

Doherty, Y., M. Harley, K. Vos, and K. Splinter. 2022. "A Python toolkit to monitor sandy shoreline change using high-resolution PlanetScope cubesats." *Environmental Modelling & Software* 157. https://doi.org/10.1016/j.envsoft.2022.105512.

Dolan R., H. Lins, B. Hayden. 1988. "Mid-Atlantic coastal storms." *Journal of Coastal Research* 4: 417–433.

Fraser, G., C. Larsen, and N. Hester. 1990. “Climatic controls of lake levels in the Lake Michigan and Lake Huron basins.” In Schneider, A.F., and Fraser, G.S., eds., *Late Quaternary history of the Lake Michigan basin: Geological Society of America Special Paper* 251, p. 75-89.

Holman, R., A. Sallenger, T. Lippmann, and J. Haines. 1993. The Application of Video Image Processing to the Study of Nearshore Processes. *Oceanography*, 6(3): 75–85.

Xiaoying, J., and R. Schafer. 2016. Method and system for automatic registration of images. Exelis, Inc., assignee; now owned by L3Harris Technologies, Inc. U.S. Patent No. 9,245,201 (issued January 26, 2016).

LeBlanc, R., and W. Hodgson. 1959. “Origin and development of the Texas shoreline.” *Gulf Coast Association of Geological Societies Transactions* 9, p. 197–220.

Lee, G., Nicholls, R., and Birkemeier, W. 1998. Storm-driven variability of the beach-nearshore profile at Duck, North Carolina, USA, 1981–1991. Marine Geology, 148, (3–4), p. 163-177, https://doi.org/10.1016/S0025-3227(98)00010-3.

Lippmann, T. and R., Holman. 1989. “Quantification of Sand Bar Morphology: A Video Technique Based on Wave Dissipation.” *Journal of Geophysical Research*, 94(C1):995–1011.

Ludka, B., R. Guza, W. O’Reilly, M. Merrifield, R. Flick, A. Bak, T. Hesser, R. Bucciarelli, C. Olfe, B. Woodward, W. Boyd, K. Smith, M. Okihiro, R. Grenzeback, L. Parry and G. Boyd. 2019. “Sixteen years of bathymetry and waves at San Diego beaches.” *Sci Data* 6, 161 https://doi.org/10.1038/s41597-019-0167-6.

Luijendijk, A., G. Hagenaars, R. Ranasinghe, F. Bart, G. Donchyts and S. Aarninkof. 2018. "The state of the world’s beaches." *Scientific reports* 8.1: 1-11.

McGill, S., B. Harris, B., McFall, D. Krafft,N. Bain, N. Olsen, N., I. Conery, and M. Chasten. 2022. “Morphological analysis of a nearshore nourishment along the Atlantic Coast of New Jersey, USA.” *Journal of Marine Science and Engineering* 10(11), 1622.

Onnink, C., 2020. Dynamic shoreline response to a shallow concentrated

nearshore Berm nourishment. Master of Science Thesis. Delft University of Technology.

Paine, J., T. Caudle, and J. Andrews, J. 2021. "Shoreline movement and beach and dune Volumetrics along the Texas Gulf Coast, 1930s to 2019." *Bureau of Economic Geology*, The University of Texas at Austin. Final report prepared for the General Land Office under Contract No. 16-201-000, Work Order No. B42 CEPRA Project No. 1662.

Scheffler D., A. Hollstein, H. Diedrich, K. Segl, and P. Hostert. 2017. "AROSICS: An Automated and Robust Open-Source Image Co-Registration Software for Multi-Sensor Satellite Data." *Remote Sensing* 9(7):676. https://doi.org/10.3390/rs9070676.

Stapor, F., and J. May. 1983. "The cellular nature of littoral drift along the northeast Florida coast." *Marine Geology* 51 (3-4), p. 217-237. https://doi.org/10.1016/0025-3227(83)90105-6.

Stockdon, H., A. Sallenger, R. Holman, and P. Howd. 2007. "A simple model for the spatially-variable coastal response to hurricanes." *Marine Geology* 238(1-4), 1–20. https://doi.org/10.1016/J.MARGEO.2006.11.004.

Storey, J., D. Roy, J. Masek, F. Gascon, and M. Choate. 2016. "A Note on the Temporary Misregistration of Landsat-8 Operational Land Imager (OLI) and Sentinel-2 Multi Spectral Instrument (MSI) Imagery." *GSCE Faculty Publications*. 35. https://openprairie.sdstate.edu/gsce_pubs/35.

Storey, M. Choate, K. Lee Landsat-8 Operational Land Imager on-orbit geometric calibration and performance Remote Sens., 6 (11) (2014), pp. 11127-11152, 10.3390/rs61111127 https://sentinel.esa.int/documents/247904/4598066/Sentinel-3-OLCI-Land-Handbook.pdf.

Trémas, T., C. Déchoz, S. Lacherade, J. Nosavan, and B. Petrucci. 2015. "Sentinel-2: presentation of the CAL/VAL commissioning phase", Proc. SPIE 9643, Image and Signal Processing for Remote Sensing XXI, 964309. https://doi.org/10.1117/12.2194847.

Thompson, E. 1977. “Wave climate at selected locations along U.S. coasts.” Tech. Rept. 77-1, Ft. Belvoir, Virginia: U.S. Army Corps of Engineers.

Tondewad, P., and D. Manisha. 2020. “Remote Sensing Image Registration Methodology: Review and Discussion.” *Procedia Computer Science*. 171. 2390-2399. 10.1016/j.procs.2020.04.259.

Theuerkauf, E., K. Braun, D. Nelson, M. Kaplan, S. Vivirito, and J. Williams. 2019. “Coastal geomorphic response to seasonal water-level rise in the Laurentian Great Lakes: An example from Illinois Beach State Park, USA.” *Journal of Great Lakes Research*, 45 (6), 1055-1068.

Velasquez-Montoya, L., M. Overton, and E. Sciaudone. 2020. Natural and anthropogenic-induced changes in a tidal inlet: Morphological evolution of Oregon Inlet. *Geomorphology* 350.

Vos, K., M. Harley, K. Splinter, J. Simmons, and I. Turner. 2019. “Sub-annual to multi-decadal shoreline variability from publicly available satellite imagery.” *Coastal Engineering* 150, 160-174.

Vos, K., M. Harley, K. Splinter, A. Walker, and I. Turner. 2020. Beach slopes from satellite-derived shorelines. *Geophysical Research Letters* 47 (14).

Xu, N., 2018. “Detecting Coastline Change with All Available Landsat Data over 1986 – 2015 : A Case 835 Study for the State of Texas , USA.” *Atmosphere (Basel)* 9, 107. 836 https://doi.org/10.3390/atmos9030107.